Very High Temperature Reactor (VHTR) Deep Burn Core and Fuel Analysis
Complete Design Selection for the Pebble Bed Reactor

B. Boer
A. M. Ougouag

September 2010

Very High Temperature Reactor (VHTR) Deep Burn Core and Fuel Analysis
Complete Design Selection for the Pebble Bed Reactor

B. Boer
A. M. Ougouag

September 2010

Idaho National Laboratory
Deep Burn Project
Idaho Falls, Idaho 83415

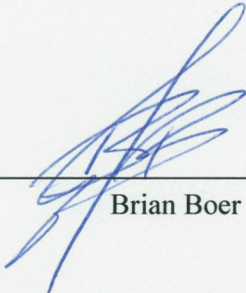http://www.inl.gov

Author:

_____
              Brian Boer   9/17/10

Reviewed by:

_____
              Michael A. Pope   9/17/10

Concurred by:

_____
(Work Package Manager)   Abderrafi M. Ougouag   9/17/10

SUMMARY

Significant Accomplishments

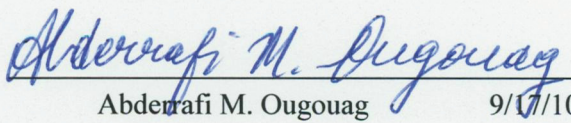- Several core design modifications of the Deep-Burn pebble-bed reactor have been investigated that lead to an improvement in the temperature reactivity coefficient. Both analytical methods and SCALE-6 were used to investigate the impact of Erbium on the temperature coefficient. The location, loading, and the Erbium particle size in the pebble have been varied to improve its effectiveness.

- To reduce power peaking in the core, SCALE-6 analyses have been performed for various core design modifications. Reduction in size and density of the inner reflector and a cylindrical core design were analyzed.

- The Deep-Burn pebble bed reactor design was optimized for discharge burnup, maximum fuel temperature, and the temperature reactivity feedback using a full-core analysis using coupled PEBBED, THERMIX, and SCALE-6 calculations. The parameters of this investigation were the heavy metal loading per pebble and the Er-167 concentration in the fuel kernel. Furthermore, two alternative core designs were considered that either adopt a neutronically 'transparent' inner reflector or a cylindrical pebble-bed core.

- The decay heat in the Deep-Burn pebble bed reactor was investigated using a detailed calculation in SCALE-6 (ORIGEN). Decay heat curves for several burnup levels were computed. Differences in the decay for two Deep-Burn fuels (with and without initial minor actinides in the fuel) were analyzed and compared to 'standard' UO_2 fuel. A typical decay heat curve was implemented in the thermal-hydraulics code THERMIX for future transient analysis.

- Transient analysis of a Depressurized Loss of Forced Cooling (DLOFC) incident in a Deep-Burn HTR-PM design was performed. The influence of the graphite conductivity, which is a function of the fast fluence, on the fuel temperature during the transient was calculated. The impact of the Deep-Burn decay heat on the fuel temperature was also computed.

- An improved model for CO formation from free oxygen has been implemented in the PASTA fuel performance code. The model is based on data provided by T. Besmann (ORNL).This data was obtained from a detailed thermo-chemical analysis of the constituents in the Deep-Burn fuel and the resulting CO (and CO_2) formation from the free oxygen. The effect of oxygen getters (SiC, ZrC) is also implemented in this model. The model is used in the PASTA stress analyses.

- Fuel performance analysis of the coated particles experiencing a DLOFC transient has been performed using the PASTA code.

- A statistical model has been implemented in the PASTA code, which has been used to compute the impact of the variation in coated particle size on the fuel performance. Furthermore, the effect of the radial location of the pebble in the core on the stress was calculated.

- A fuel performance inter-comparison has been carried out by the cooperating institutions (Idaho National Laboratory [INL], KAERI, GA) within the workscope of the Deep Burn Project, using a set of pre-defined TRISO conditions (burn-up level, temperature and power level, etc.) and the outcome is tabulated. The areas of agreement between the PASTA, COPA and PISA codes are pointed out and the areas that require further modeling or reconciliation are shown. The sensitivity of several of the input parameters has been investigated.

Publications

The following papers have been published as a result of the studies presented in this document:

- Boer, B. and A.M. Ougouag (2010) "Core analysis, design and optimization of a Deep-Burn pebble bed reactor," PHYSOR 2010 – Advances in Reactor Physics to Power the Nuclear Renaissance, Pittsburgh, Pennsylvania, USA, May 9–14, 2010, American Nuclear Society, LaGrange Park, Illinois (2010).

- Boer, B. and A.M. Ougouag (2010) "Stress analysis of coated particle fuel in the Deep-Burn pebble bed reactor design," PHYSOR 2010 – Advances in Reactor Physics to Power the Nuclear Renaissance, Pittsburgh, Pennsylvania, USA, May 9–14, 2010, American Nuclear Society, LaGrange Park, Illinois (2010).

- Boer, B. and A.M. Ougouag (2010) "Core Optimization of a Deep-Burn Pebble Bed Reactor," Proceedings of ICAPP '10, (Paper #10290), San Diego, California, USA, June 13–17, 2010.

The following paper has been accepted for publication as a result of the studies presented in this document:

- Boer, B., Y. M. Kim, W. Wu, A. M. Ougouag, D. McEachern, and F. Venneri (2010)"Inter-comparison of Computer Codes for TRISO-based Fuel Micro-Modeling and Performance Assessment," HTR 2010 Conference Prague, paper 159, Czech Republic, October 18–20, 2010.

CONTENTS

FIGURES

TABLES

Very High Temperature Reactor (VHTR) Deep Burn Core and Fuel Analysis
Complete Design Selection for the Pebble Bed Reactor

xii   9/21/2010

ACRONYMS

BAF	Bacon Anisotropy Factor
BONAMI	Bondarenko method
BP	burnable poison
CB	core barrel
CENTRM	Continuous ENergy TRansport Module
CHOPS	Compute HOmogenized Pointwise Stuff
CSAS5	Control module for enhanced Criticality Safety AnalysiS with KENO V.A
DB	Deep-Burn
DLOFC	depressurized loss of forced cooling
DOE	Department of Energy
ENDF/B-VII	Evaluated Nuclear Data File
FIMA	fissions per initial metal atom
FTC	fuel temperature coefficient
HM	Heavy Metal
HTR-PM	High Temperature Gas-Cooled Reactor-Pebble bed Module
IHM	initial heavy metal
INL	Idaho National Laboratory
IPyC	inner pyrolytic carbon
LOFC	Loss of Forced Cooling
LWR	light water reactor
MTC	moderator temperature coefficient
NEA	Nuclear Energy Agency
OECD	Organization for Economic Co-operation and Development
OPyC	outer pyrolytic carbon
PBMR	Pebble Bed Modular Reactor
PBR	pebble bed reactor
PMC	Produce Multigroup Cross sections
RHRS	reactor heat removal system
RPV	reactor pressure vessel
SCALE-6	A Modular Code System for Performing Standardized Computer Analyses for Licensing Evaluation
SiC	silicon carbide
TRISO	tri-isotopic

xiv

Very High Temperature Reactor (VHTR) Deep Burn Core and Fuel Analysis
Complete Design Selection for the Pebble Bed Reactor
9/21/2010

TRU   transuranic

UTC   uniform temperature coefficient

VERY HIGH TEMPERATURE REACTOR (VHTR) DEEP BURN CORE AND FUEL ANALYSIS

COMPLETE DESIGN SELECTION FOR THE PEBBLE BED REACTOR

1.   INTRODUCTION

The Deep-Burn (DB) concept [1] focuses on the destruction of transuranic nuclides from used light water reactor (LWR) fuel. These transuranic nuclides are incorporated into tri-isotopic (TRISO) coated fuel particles and used in gas-cooled reactors with the aim of a fractional fuel burnup of 60 to 70% in fissions per initial metal atom (FIMA). This high performance is expected through the use of multiple recirculation passes of the fuel in pebble form without any physical or chemical changes between passes. In particular, the concept does not call for reprocessing of the fuel between passes. In principle, the DB pebble bed concept employs the same reactor designs as the presently envisioned low-enriched uranium core designs, such as the 400 MW_{th} Pebble Bed Modular Reactor (PBMR-400) [2].

Although it has been shown in the previous Fiscal Year (FY) (2009) that a PuO_2 fueled pebble bed reactor concept is viable, achieving a high fuel burnup while remaining within safety-imposed prescribed operational limits for fuel temperature, power peaking, and temperature reactivity feedback coefficients for the entire temperature range, is challenging. The presence of the isotopes ^{239}Pu, ^{240}Pu, and ^{241}Pu that have resonances in the thermal energy range significantly modifies the neutron thermal energy spectrum as compared to a standard, UO_2-fueled core. Therefore, the DB pebble bed core exhibits a relatively hard neutron energy spectrum. However, regions within the pebble bed that are near the graphite reflectors experience a locally softer spectrum. This can lead to power and temperature peaking in these regions. Furthermore, a shift of the thermal energy spectrum with increasing temperature can lead to increased absorption in the resonances of the fissile Pu isotopes. This can lead to a positive temperature reactivity coefficient for the graphite moderator under certain operating conditions.

Regarding the coated particle performance, the FY 2009 investigations showed that no significant failure is to be expected for the reference fuel particle during normal operation. It was found, however, that the sensitivity of the coating stress to the CO production in the kernel was large. The CO production is expected to be higher in DB fuel than in UO_2 fuel, but its exact level has a high uncertainty. Furthermore, in the fuel performance analysis transient conditions were not yet taken into account.

The effort of this task in FY 2010 has focused on the optimization of the core to maximize the pebble discharge burnup level, while retaining its inherent safety characteristics. Using generic pebble bed reactor cores, this task will perform physics calculations to evaluate the capabilities of the pebble bed reactor to perform utilization and destruction of LWR used-fuel transuranics. The task will use established benchmarked models, and will introduce modeling advancements appropriate to the nature of the fuel considered (high transuranic [TRU] content and high burn-up).

The following section will describe the reference Deep-Burn pebble-bed reactor design in detail. In the section after that the goals of the project of Fiscal Year 2010 are stated.

1.1   The Deep-Burn Pebble-bed Reactor Concept

The initial Deep-Burn Pebble-Bed Reactor design is based on the PBMR-400 reactor design. The physical layout of the PBMR-400 is illustrated in Figure 1 and key parameters are given in Table 1. The design features inner and outer graphite radial reflectors embedding an annular core of slowly downward-flowing pebbles. The mode of operation of the PBMR-400 is that of (nearly) continuous online reloading and of recirculation of pebbles on multiple passes until the target burnup is reached. The simplified DB PBR initial reactor design is similar to the one described in the OECD/NEA PBMR-400 Benchmark [3].
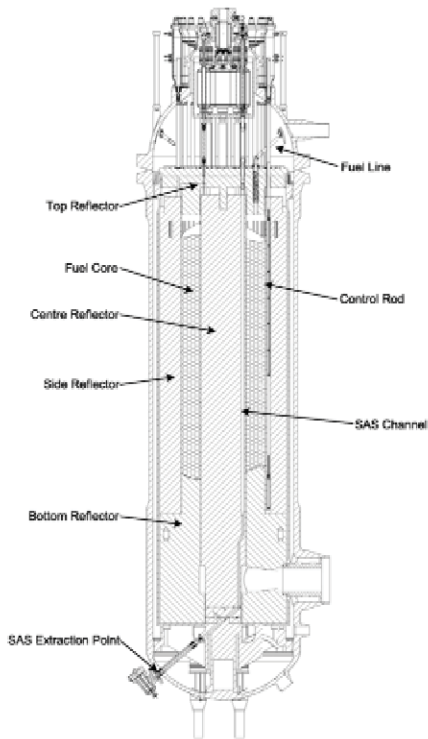
Figure 1. Overview of the Pebble Bed Modular Reactor 400 MW$_{th}$ design.

The simplified reactor model assumes azimuthal symmetry resulting in a two-dimensional (r,z) model reactor. The top cones (or conuses) that result from the fueling process in which pebbles are dropped into the core is ignored (i.e., assumed flat). Similarly, the bottom cone-shaped fuel regions at the fuel discharge openings are assumed flat. Pebble flow patterns within the core region are assumed to remain within parallel vertical virtual channels. The pebbles flow at a constant speed throughout the core. Control rods in the side reflector are modeled as an annular cylindrical layer or grey curtain of specified a given ^{10}B concentration. Consequently a uniform vertical flow velocity distribution of the pebbles over the entire radius of the core is assumed. Figure 2 shows the material layout and the simplified geometry of the reactor design that has been used in the analyses.

Table 1. Major design and operating characteristics of PBMR-400 design.

PBMR Characteristic	Value
Installed thermal capacity	400 MW(t)
Installed electric capacity	165 MW(e)
Core configuration	Vertical with fixed centre graphite reflector
Fuel	TRISO coated DB-fuel in graphite spheres

PBMR Characteristic	Value
Primary coolant	Helium
Primary coolant pressure	9.0 MPa
Moderator	Graphite
Core outlet temperature	900°C
Core inlet temperature	500°C
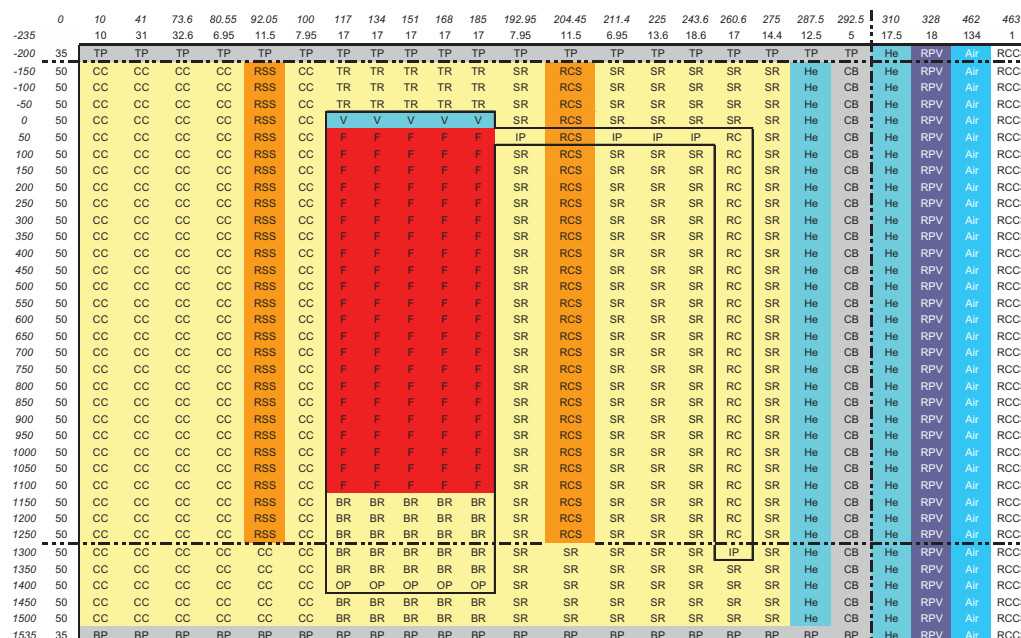
CORE LAYOUT DEFINITIONS

F	REACTOR CORE CONTAINING THE FUEL
V	HELIUM GAP BETWEEN FUEL AND TOP REFLECTOR: VOID
CC	CENTRAL REFLECTOR: GRAPHITE
TR	TOP REFLECTOR: GRAPHITE
BR	BOTTOM REFLECTOR: GRAPHITE
SR	SIDE REFLECTOR: GRAPHITE
RCS	REACTOR CONTROL SYSTEM CHANNEL : GRAPHITE / GREY CURTAIN AREA
RSS	RESERVE SHUTDOWN SYSTEM CHANNEL : GRAPHITE / GREY CURTAIN AREA
IP	INLET PLENUM TOP / BOTTOM : GRAPHITE
RC	RISER CHANNEL IN SIDE REFLECTOR : GRAPHITE
OP	OUTLET PLENUM BOTTOM : GRAPHITE
He	STAGNANT HELIUM
TP	TOP PLATE : IRON : ADIABATIC BOUNDARY
BP	BOTTOM PLATE : IRON : ADIABATIC BOUNDARY
CB	CORE BARREL : IRON
RPV	REACTOR PRESSURE VESSEL : IRON
Air	STAGNANT AIR
RCCS	REACTOR CAVITY COOLING SYSTEM : 20C TH BOUNDARY
- · - · -	NEUTRONIC BOUNDARY BONDITIONS

Figure 2. PBMR-400 neutronics and thermal-hydraulics reactor model.

Two fuel types have been considered in the present analysis (see Table 2). In the first type only the Pu isotopes from LWR used fuel are used. In the second type some of the neptunium and americium isotopes are also extracted from the LWR fuel. The DB TRISO particles have a PU/MA O_{2-x} kernel at their very

Very High Temperature Reactor (VHTR) Deep Burn Core and Fuel Analysis
Complete Design Selection for the Pebble Bed Reactor
9/21/2010

4

center (see Figure 3 and Table 3) inner pyrolytic carbon (IPyC) layer, a silicon carbide (SiC) layer, and an outer pyrolytic carbon (OPyC) layer. These coatings provide the primary containment of the fission products that are generated in the fuel kernel.

Table 2. The compositions of the two Deep-Burn fuel types considered in the analyses.

Fuel kernel	Fuel loading
Pu fuel	2.6% ^{238}Pu, 54% ^{239}Pu, 24% ^{240}Pu, 13% ^{241}Pu, 6.8% ^{242}Pu
Pu + MA fuel	6.8% ^{237}Np, 2.9% ^{238}Pu, 49% ^{239}Pu, 23% ^{240}Pu, 8.8% ^{241}Pu, 4.9% ^{242}Pu, 2.8% ^{241}Am, 0.02% ^{242m}Am, 1.4% ^{243}Am

Figure 3. TRISO coated particle under microscope.
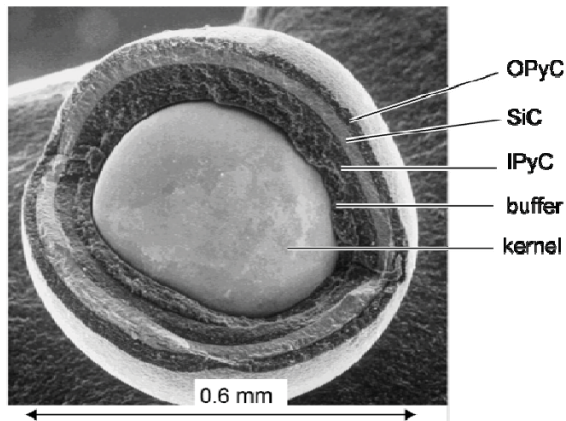
Table 3. Deep-Burn TRISO coated particle dimensions.

Layer	Thickness [μm]
Kernel	200 (diameter)
C buffer	90
IPyC	40
SiC	35
OPyC	40

1.2 Fiscal Year 2010 Tasks for the Deep-Burn Pebble-bed Reactor Concept

The main task is the optimization of the Deep Burn pebble bed reference design. The main challenges with the reference design that were identified in FY 2009 were:

1. A positive temperature reactivity coefficient for the graphite moderator at low temperatures and high fuel burnup.

2. High power and temperature peaking at the core regions that are next to the graphite reflectors.

3. Small margins in the coating stress of the DB TRISO particle and significant failure during anticipated loss of forced cooling (LOFC) transients. Furthermore, the formation of CO could lead to increased fuel failure.

The above stated challenges have been addressed, resulting in a new DB pebble bed reference design, in which the following constraints had to be met:

1. Reactor power of 200–600 MW

2. Helium outlet temperature of 750–900°C

3. Negative temperature coefficients for the entire temperature range and for the entire core

4. High fuel burnup >550 MWd/kg

5. Low fuel failure for all anticipated conditions ($<5 \times 10^{-5}$).

The analysis and design of the improved reactor concept has been split into two tasks. The first task focuses on the core, while the second deals with the performance of the coated particle fuel. The two main tasks are in turn split up in the following subtasks:

1. Analysis and design of the Deep-Burn pebble-bed core

Subtask 1.1: Improvement of the temperature reactivity coefficient

To improve the moderator temperature coefficient both the addition of Er-167 to the pebble or fuel kernel as well as an increasing the fuel loading per pebble have been considered. Furthermore, effect of the location within the pebble or coated particle fuel of the Er-167 on the temperature coefficient has been investigated.

Subtask 1.2: Reduction of the power and temperature peaking in the core

To reduce the power and temperature peaking in the core near the inner and outer reflectors, the dimensions and the reflector graphite density have been modified.

Subtask 1.3: Analysis of the decay heat from Deep-Burn fuel

The decay heat from plutonium and minor actinide fuel is expected to be higher after several hours of reactor shut-down as compared to uranium fuel. The impact on the fuel temperature during a LOFC transient is investigated.

Subtask 1.4: Analysis of the sensitivity of the fuel temperature on the fast neutron dose

The fast neutron flux level (E > 0.1 MeV) is expected to be higher in a Deep-Burn core than in a uranium fueled reactor. The thermal conductivity of graphite, present in both the pebble fuel and the reflectors, is dependent on the fast fluence level. The impact of the fluence level on the fuel temperature during normal and LOFC conditions has been determined.

2. Analysis and design of the Deep-Burn coated particle fuel

Subtask 2.1: Investigation of the impact of CO production and oxygen getter on the particle performance

In the stress analysis of FY 2009, it was found that the internal pressure and the resulting coating stresses are highly impacted by the production of CO by free oxygen. The PASTA code has been updated with recently published thermo-chemical data for CO production, which is used in the new analysis. Furthermore, the effect of using an oxygen getter on the stresses is quantified.

Subtask 2.2: Investigation of the impact of the variation in the thicknesses of the particle coatings on the performance

In reality, the size of the coated particles will slightly deviate from the prescribed one as a result of the fabrication process. Therefore, a statistical analysis of the variation of the particle dimensions and resulting failure probability of particles has been conducted.

Subtask 2.3: Transient analysis of the fuel performance during an LOFC incident

During an LOFC event in the reactor the fuel temperatures in some core regions are considerable higher than during normal operation. This might result in an increase of the coating stresses and resulting particle failure. An investigation of the impact of a temperature increase on the fuel performance has therefore been performed.

Subtask 2.4: Inter-comparison of fuel performance codes fuel coated particle stress analysis

From the above subtasks a new DB particle fuel design is analyzed. The results of three fuel performance codes for the design are compared. The differences in the results have been analyzed and a sensitivity

6

Very High Temperature Reactor (VHTR) Deep Burn Core and Fuel Analysis
Complete Design Selection for the Pebble Bed Reactor
9/21/2010

analysis on the input parameters has been performed. These analyses quantify the uncertainty in the performance of the new particle design.

2.   OVERVIEW OF THE CODE SYSTEM FOR ANALYSIS OF THE DEEP-BURN PEBBLE-BED REACTOR CORE AND FUEL

In the following two sections, the code systems for analysis of pebble-bed reactor cores and fuel are described, respectively.

2.1   Code System for Analysis of Pebble-bed Reactor Cores

A code-to-code coupling between PEBBED [4] and SCALE-6 [5] has been implemented, which allows PEBBED to read microscopic neutron cross sections in AMPX format generated with the CSAS5 module of SCALE-6. The fine (238) energy group structure from ENDF/B-VII is collapsed for this purpose to a broad group structure (12 groups, of which 7 are thermal) to be used in PEBBED. Thermal-hydraulic feedback is provided by the THERMIX(-KONVEK) code [6], which is a built-in routine of PEBBED. Short descriptions of the PEBBED code, the cross section generation procedure in SCALE-6, and the THERMIX code are given in the following sections.
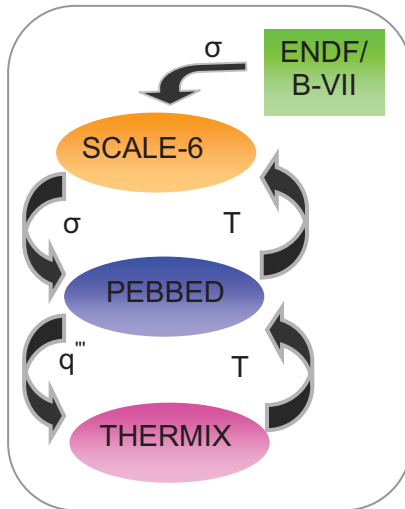
Figure 4. Pebble-bed core analysis code system overview.

2.1.1   Description of the PEBBED Code

The PEBBED code [4] is a tool for analyzing the asymptotic fuel cycle in recirculating pebble bed reactors. Equations for neutron flux and nuclide distribution in a pebble-bed core are solved self-consistently via an iterative scheme. The neutronics solver uses either a standard finite difference technique or a nodal diffusion method. The burnup solver uses a semi-analytical method that guarantees convergence and accuracy. A key step in the algorithm is the computation of the entry plane density of each nuclide of interest in each axial pebble flow channel. These values depend upon the pebble loading and recirculation policy and the burnup accrued by pebbles on successive passes through the core. The current iterate of the flux is used to compute the exit plane nuclide density in a pebble after one pass through the core in each channel, based on the density of that nuclide in a fresh pebble. Pebbles are then distributed according to the recirculation scheme to generate the entry plane density in each channel on the following pass. This is repeated until the pebbles meet or exceed the discharge cutoff burnup. The exit plane values are then averaged according to the recirculation scheme in order to produce the actual entry plane nuclide densities.

2.1.2   Cross Section Generation Procedure using SCALE-6

The Criticality Safety Analysis Sequences (CSAS)(6) module from Standardized Computer Analyses for Licensing Evaluation (SCALE)-6 [5] has been used for the calculation of reactivity coefficients and to generate the neutron cross sections for PEBBED. The cross section generation method used here is largely based on a benchmarked SCALE-6 procedure [7]. In this method two lattice cell calculations are performed: (1) a fuel kernel surrounded by coating material and graphite matrix is treated; and (2) a graphite matrix containing TRISO fuel and graphite (which is surrounded by a graphite shell and helium) is used in an infinite lattice calculation. The resonance treatment has been performed using the Bondarenko method (BONAMI) for the unresolved resonances range and using the SCALE modules CENTRM/PMC/CHOPS for the resolved resonances. CENTRM solves the 1-D transport equation using point wise cross sections to calculate the corresponding point wise spectrum. PMC uses the point wise cross sections, the CENTRM-calculated point wise spectrum, and the multigroup data (where point wise spectrum is not calculated) and generates resonance-corrected multigroup cross sections. Note that the NITAWL module, which uses the Nordheim Integral Method, is omitted here.

The double heterogeneity (caused by shadowing effects of the fuel particles and fuel zones of the pebbles) is treated by first calculating the point-wise flux disadvantage factors for the particle-matrix unit cell and then using these factors to create the homogenized point-wise particle/matrix mixture cross sections. The homogenized point-wise cross sections are then used in the second pass to create the final resonance-shielded multigroup cross sections that represent the fuel pebbles. Finally, deterministic calculations have been performed for the given cell (TRISO or pebble) with the one-dimensional Discrete Ordinates code XSDRNPM. In this eigenvalue calculation a white boundary condition is used on the outer surface.

During a PEBBED calculation, the SCALE-6 input files are updates for local temperature and burnup. To this end 90 different material zones have been defined and 55 of which are in the pebble bed region of the reactor (core zone is divided into 5 radial and 11 axial zones), 4 for the control rod, 1 for the void region, and the remaining 30 are for the reflector regions. The void region on top of the pebble bed was modeled by directional diffusion coefficients. The control rod was modeled by using an equivalent boron concentration. A simplification to the model was made by modeling the side void (air gap) and reactor pressure vessel as graphite.

It was chosen to perform the PEBBED full core calculation in a high number of energy groups (12), since intermediate calculations between pebble level and full core calculations are omitted. Furthermore, the depletion calculation in PEBBED uses the zone wise energy spectrum of the full core calculation to perform the zone wise depletion. Therefore, it is attractive to retain in a relatively fine group energy structure, especially in the case of Pu fuel with important low-lying resonances.

2.1.3   Description of the THERMIX Code

The thermal-hydraulic feedback is provided by THERMIX-KONVEK [6], which utilizes the power density profile calculated by PEBBED and computes the average temperature for each material zone. This temperature is then used in the cross section preparation step in SCALE-6 in which each zone is treated separately.

THERMIX is a 2-D thermal hydraulics code that consists of a heat conduction (and thermal radiation) part and a part for the fluid convection. In the first, the pressure field of the moving fluid for a 2-D cylindrical configuration is solved by linking the equations for conservation of mass and momentum. In the second part of the code the energy conservation equation is solved for steady state or time-dependent cases considering the solid material. The two parts are coupled by a source term that represents the heat transfer between the solid and the fluid.

The pebble bed is treated as a (porous) homogeneous material, having an effective conductivity based on the Zehner-Schlünder relation. In this relation not only conductivity through touching pebbles is taken into account, but also radiation between the pebbles and a convective effect caused by mixing of the helium fluid in the direction perpendicular to the flow direction.

At the boundary of the conduction model a fixed temperature (side) or an adiabatic boundary condition (top and bottom) is prescribed. For the convection model, the coolant inlet temperature and outlet pressure are used as boundary conditions.

2.2   Code System for Stress Analysis of Coated Particle Fuel in Pebble-bed Reactors

A schematic overview of the PEBBED-PASTA code system is given in Figure 5. In this calculation scheme the PEBBED code is used to calculate the environmental parameters of the fuel particles thus providing the boundary conditions for the stress analysis performed with the PASTA code.
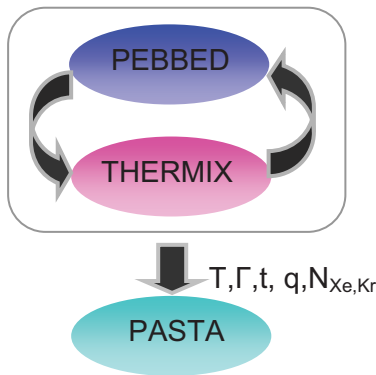
Figure 5. Fuel performance code system overview.

The following data are provided by PEBBED and read into PASTA for the analysis for each axial and radial core position and for each pebble core pass (Figure 5):

T: The temperature of the fuel. PEBBED provides the average fuel, average pebble center, and pass-dependent pebble-center fuel temperature histories, which can be used in separate stress analysis evaluations.

Γ: The fast neutron fluence (E > 0.1 MeV), which is calculated with PEBBED from a 28 group energy group structure used for the full core calculation.

q''': The power density history can be read for use in reconstructing the fuel kernel temperature; the PASTA code can use this information to perform sampling over the temperature profile in the fuel zone of the pebble.

B: The burnup level of the fuel.

t: The residence time of the pebble in the core.

$N_{Xe,Kr}$: The production rate of the stable gaseous fission products of Xe and Kr (^{83}Kr, ^{84}Kr, ^{85}Kr, ^{86}Kr, ^{131}Xe, ^{132}Xe, ^{134}Xe, ^{136}Xe) within the kernel.

The PASTA code [8,9] describes the mechanical behavior of TRISO particles during irradiation and aims at calculating the coating stresses and the corresponding failure probabilities.

PASTA embodies a one-dimensional analytical and multi-layer model that takes into account the visco-elastic behavior of the coating layers and the surrounding graphite during irradiation. The main source of stress in all layers is due to the pressure build-up from the gaseous fission products in the buffer layer resulting in a radial stress on the IPyC. Moreover, the Pyrocarbon (IPyC and OPyC) layers exhibit radiation-induced dimensional changes and creep (in the radial and tangential directions). Finally, the model allows thermal expansion of all layers. PASTA solves the general stress strain equations to determine the stresses in the coating layers. In PASTA, the mechanical failure probability of the coated particle is determined by the magnitude of the (tensile) stress in the SiC layer, which is the main load-bearer, according to the following Weibull distribution:

$$\Psi = 1 - \exp\left(-\ln(2) \left(\frac{\sigma_t}{\sigma_{med}} \right)^m \right) \tag{1}$$

in which σ_t is the tangential (tensile) stress in the SiC layer, σ_{med} the median strength of the SiC, and m is the Weibull modulus of the SiC strength, which are taken to be $\sigma_{med} = 340$ MPa and $m = 5$ from Snead et al.'s article [10].

Gaseous fission products (Xe and Kr) accumulate during irradiation in the buffer layer and induce a pressure buildup that depends on the kernel temperature and buffer volume.

The buildup of gaseous fission products can be calculated both analytically and numerically by solving the time-dependent fission product diffusion equation:

$$\frac{\partial C}{\partial t} = \frac{D(T)}{r^2} \left[\frac{\partial}{\partial t} \left(r^2 \frac{\partial C}{\partial r} \right) \right] + \beta \tag{2}$$

in which β is the production of fission products calculated by PEBBED and depends on the irradiadition history, $D(T) [s^{-1} m^2]$ is the temperature-dependent diffusion coefficient, which can be calculated with [11] (assuming Xe and Kr as the fission products):

$$D'(T) = 5.10^{-3} e^{\left(-\frac{Q}{RT} \right)} \tag{3}$$

with $D' = \frac{D}{r^2}$, $Q = 155.4 \ 10^3$ J/mol and $R = 8.314$ J/mol/K.

In the PASTA code both a numerical method using a finite difference scheme as well as an analytical method for the calculation of the fractional release F of fission products from the kernel to the buffer can be used. The (approximate) analytical solution for F using Equations (2) and (3), assuming a zero concentration at the kernel surface, is as follows [12]:

$$F^k(t) = 1 - \sum_{n=1}^{\infty} \left[\frac{6a^2}{n^4 \pi^4} \sum_{s=1}^{k} \frac{\beta^s}{D^s} \left(1 - e^{-\phi^s} \right) \times e^{-\Delta\Phi^{ks}} \right] \times \left[\sum_{s=1}^{k} (\beta t)^s \right]^{-1} \tag{4}$$

in which $F^k(t)$ is the release-to-birth ratio of the fission gases at cycle k, $\phi = n^2 \pi^2 \left(Dt / a^2 \right)$ and $\Delta\Phi^{ks} = \sum_{r=s}^{k} \phi^r$ and n is chosen to provide both fast calculations and good accuracy.

Besides direct formation of gaseous fission products, formation of CO gas by a reaction of the oxygen present in the fuel kernel and carbon in the buffer layer is possible. CO production is calculated with the

PASTA code as a function of the burnup and the temperature through interpolation of data from Besmann's article [13].

The resulting pressure (from both fission products and CO production) on the IPyC layer is calculated as a function of the kernel temperature and the buffer volume with the Redlich Kwong equation of state [14]:

$$RT = \left(p + \frac{a}{T^{\frac{1}{2}} V_m (V_m + b)} \right) (V_m - b) \tag{5}$$

The ideal gas law is omitted here, because it underpredicts the pressure significantly.

The PyC coating layers exhibit a dimensional change under irradiation of fast neutron flux. The relations for the dimensional change for the radial and tangential direction of the layers are adopted from Ho's report [15]. The correlation is a function of the Bacon Anisotropy Factor (BAF) [16] and the temperature.

Pyrocarbon and graphite materials creep under irradiation, partly reducing the stress. For the pyrocarbon layers a value of 2.0×10^{-29} (MPa.m^{-2})$^{-1}$ (for the creep coefficient) was adopted from literature [17].

Thermal expansion of the PyC layers is adopted in the model and the thermal expansion coefficients are taken from Wang's thesis [18]:

$$\alpha_r = \left[\frac{-250}{6 + 3 \cdot BAF} + \frac{100}{3} \right] \times 10^{-6} \tag{6}$$

$$\alpha_t = \left[\frac{40}{(2 + BAF)^2} + \frac{10}{9} \right] \times 10^{-6} \tag{7}$$

Note that for $BAF = 1$, $\alpha_r = \alpha_t = 50/9 = 5.6 \ 10^{-6}$ [K^{-1}].

3.   CORE ANALYSIS AND OPTIMIZATION OF THE DEEP-BURN PEBBLE-BED REACTOR

In the FY 2009 analysis, the performance of the reference DB pebble-bed reactor (PBMR-400) was computed. A schematic overview of the reactor design and its nominal flux, power, and fuel temperature profiles are given in Figure 6.

| (a) | (b) | (c) | (d) |
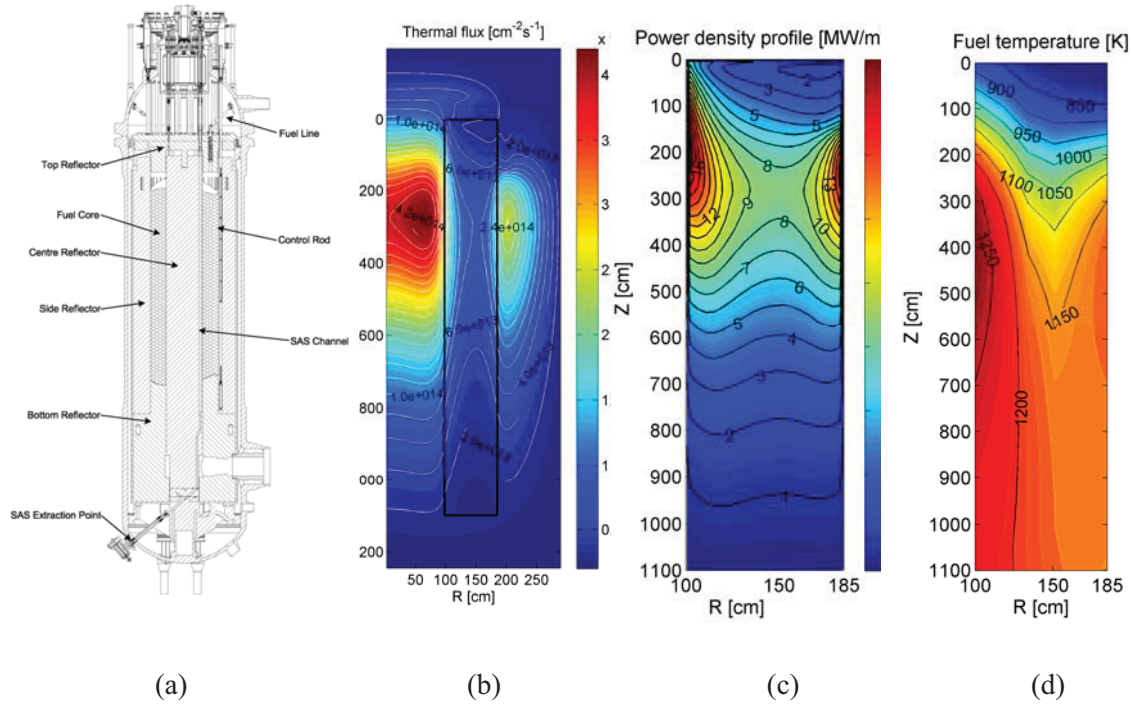
Figure 6. (a) The PBMR-400 core design, (b) the thermal flux profile, (c) the power profile; and (d) the fuel temperature profile in the DB core. Thermal flux peaking near the inner and outer reflector results in power density and temperature peaking.

Figure 6(b) shows the thermal flux profile in the Pu-fueled (equilibrium) core. The peaks in the thermal flux profile in the inner and outer reflector result in peaks in the power density profile (Figure 6[c]) and fuel temperature (Figure 6[d]) near the reflector edges. Note that the maximum core temperature (1284 K) is located below the power peak of 17.7 MW/m^3 near the inner reflector, since the coolant flow direction is downward. Note that the temperature of an individual pebble with a low fuel burnup in this region of the core can exhibit higher temperatures (1541 K) than the average pebble.

For Pu and Pu + minor actinide (MA)-fueled pebble reactor designs, it was found that the moderator temperature coefficient (MTC) is positive for low temperatures (T < 800 K) and high burnup values (B > 300 MWd/kg Heavy Metal [HM]). Since the fuel temperature coefficient (FTC) is small over the entire range of temperatures and burnup values, the uniform temperature coefficient (UTC) is dictated by the MTC.

The following sections present the core optimization studies performed to improve the temperature coefficient (Section 3.1) and to reduce the power and temperature peaking (Section 3.2).

3.1 Improvement of the Temperature Coefficient

3.1.1 Description of the Methodology for Analyzing the Temperature coefficients

A scoping study has been performed in which the temperature coefficient was calculated for several fuel loadings per pebble and the Erbium concentration in the kernel. A fixed temperature of 500 K has been used as well as a fixed nuclide composition set as a function the fuel burnup. For the most promising cases detailed full core coupled neutronics, thermal-hydraulics, and depletion calculations have been performed. The zone average nuclide compositions from these latter calculations have been used to calculate the temperature coefficient as a function of the core position and the temperature.

Er-167 has a large resonance at 0.5 eV, near the Pu-239 and Pu-241 resonances at 0.3 eV (Figure 7), which are important during a spectral shift, in addition to the increased absorption in the resonances with increasing temperatures (Doppler effect).
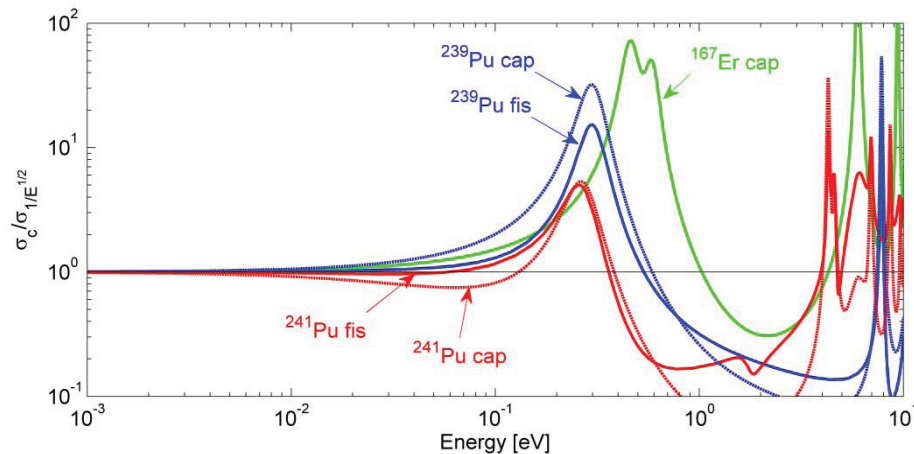
Figure 7. Capture and fission sections of Pu-239 and Pu-241 and the capture cross section of Er-167 (normalized to their $\dfrac{1}{\sqrt{E}}$ limit). The location of the Er-167 resonance near the resonances of the Pu isotopes results reduces the positive effect reactivity effect of a spectrum shift to higher energies.

The addition of Erbium to the fuel can therefore lead to an improvement of the moderator temperature coefficient. In principle the burnable poison can be added in several different ways:

1. In the kernel itself, mixed with the fuel.

   + The burnable poison will shield the fuel in the beginning of its life resulting in a more gradual depletion of the fuel and reducing the high peak in the pebble power history typical for DB fuel.

2. At the center of the fuel kernel.

   + The fuel shields the burnable poison in the beginning of life. As a result, the burnable poison 'lives' longer and has an effect on the UTC at high burnups (i.e., where it is most desired). To improve the shielding by the fuel the fuel+BP particle should be made larger than the standard one.

3. At the surface of the fuel kernel.

   + The BP shields the fuel in the beginning of life thereby reducing the power peak.

   - The BP burns faster than Case 1 and 2 since it is not shielded by the fuel and its impact on the UTC at higher burnup is smaller.

4. As a separate (second) particle in the matrix.

   + The size of the BP particle can be varied to tailor its self-shielding to achieve a larger effect on the UTC at high burnup levels.

   - Minimal shielding by the fuel.

5. In a separate pebble.

   + A high degree of freedom in BP particle size and loading.

3.1.2 Impact of the Erbium Particle Size on the Temperature Coefficient

The radius of an Er-167 particle can be optimized to yield the highest possible Doppler effect, following the theory presented in Bende's document [19]. The Doppler coefficient of reactivity can be written as:

$$\alpha_D = \ln(p)\left[\frac{1}{I_{eff}}\frac{dI_{eff}}{dT}\right] \tag{8}$$

with p as the resonance escape probability and I_{eff} as the effective resonance integral. For a fixed p, the Doppler coefficient of reactivity is a function of the Doppler coefficient $\dfrac{1}{I_{eff}}\dfrac{dI_{eff}}{dT}$. The Doppler coefficient can be maximized as a function of the particle radius using the following equation [20]:

$$\left(N_A \bar{l}_F'\right)^{-1} \approx \sigma_0 \frac{\Gamma_\gamma}{\Gamma}\left[0.21\Gamma\sqrt{\frac{A}{4E_0 k_B T}} - 0.19\right] - \sigma_p^{NRIM} \tag{9}$$

Here, N_A is the nuclide density of the absorber isotope, E_0 is the resonance energy, A is the atomic mass number, $k_B T$ is the fuel temperature in eV, σ_0 is the total cross section of the Breit-Wigner cross section at the resonance energy, Γ is the total natural line width of the resonance, Γ_0 in the natural line width for capture, σ_p^{NRIM} is the scattering cross section per absorber atom of the moderator admixed in the fuel, and $\bar{l}_F'$ is the mean-corrected cord length determined as follows:

$$\bar{l}_F' = \frac{4}{3}r_F\left(\frac{1}{A} + \frac{C}{1-C}\right) \tag{10}$$

with r_F the particle radius, A the Bell-factor (1.16), and C the Dancoff factor.

For resonance absorbers U-238, Th-232, or Er-167 in the above equation leads to optimal radii of $\bar{l}_F' = 4$ .10^{-2} cm, 4.10^{-1} cm, and $2.5.10^{-3}$ cm, respectively. As a rule of thumb, take $\bar{l}_F' = 2.5\ r_F$.

Apparently to optimize the Doppler coefficient, an absorber particle needs to be somewhere between 'black' and 'white' having a maximal impact of the local energy dependent flux, which results in a large Doppler.

However, this theory is based on the lowest lying resonance(s) of a single isotope assuming slowing down of the neutrons (1/E spectrum). It is noted that the lowest resonance of Er-167 is in the thermal range, in which there is upscattering, and that part of the resonance is shielded by the Pu-239,240,241 resonances in the DB fuel.

3.1.3   Impact of Fuel and Erbium Loading on the Temperature Coefficient

In the FY 2009 investigation of the UTC, it was found that the maximum value occurred at a temperature of around 500 K. A scoping study has been performed to investigate the UTC at this temperature with the fuel and Erbium loading as the parameters. A fixed data set for the nuclide densities as a function of the burnup was used in this study. The geometry has been simplified to a one-dimensional radial slice of the core, for which a transport calculation is performed using XSDRNPM.

It is noted that in the studies of Sections 3.1.3 and 3.1.4 the free-gas approximation for collisions in the thermal energy range of carbon was assumed for graphite. In the following full core analysis of Section 3.1.5, additional $S(\alpha,\beta)$ thermal moderator data for graphite was adopted. No significant differences in the trends were observed between the simplified and the full core studies.

Figure 8 shows the results for the UTC at various burnup levels. It can be seen that the UTC can be rendered negative if either the fuel loading or the Erbium loading is increased (or a combination of both).

Figure 9 shows the corresponding k_{eff} for the various loadings of fuel and Erbium. It can be seen that the optimal fuel loading with regard to the core reactivity is lower than the reference 2g per pebble. Low fuel loadings however result in a positive UTC (Figure 8). This cannot be compensated by increasing the Erbium loading, since this will result in too much parasitic absorption (low k_{eff}).

(a)

(b)

(c)

(d)

(e)
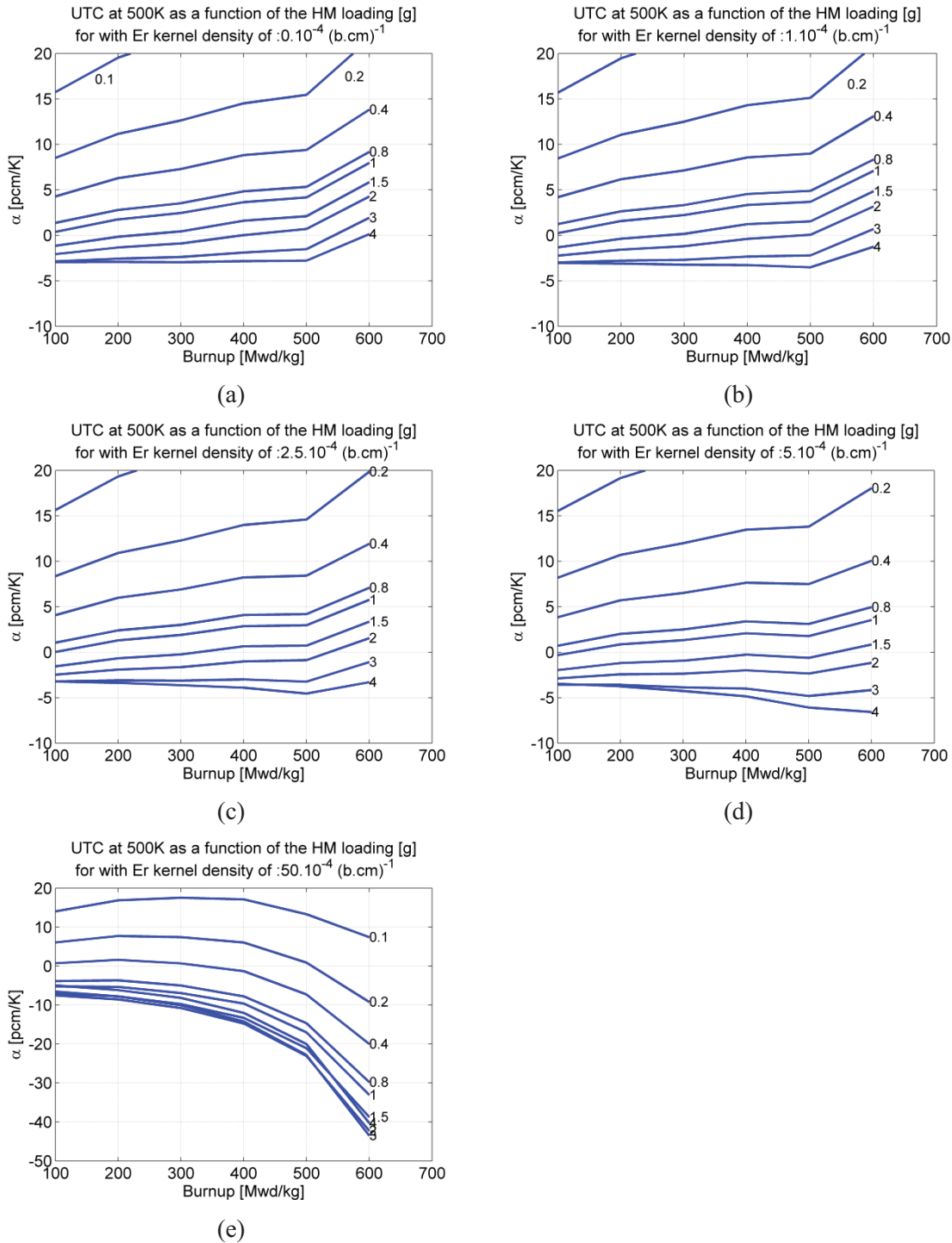
Figure 8. Impact of Er-167 densities on the UTC as a function of the fuel burnup and the HM loading per pebble [g] at 500 K. It can be seen that an Er-167 kernel density of 5.0 10^{-4} results in a negative UTC for the entire burnup range at a HM loading of 2 g/pebble.
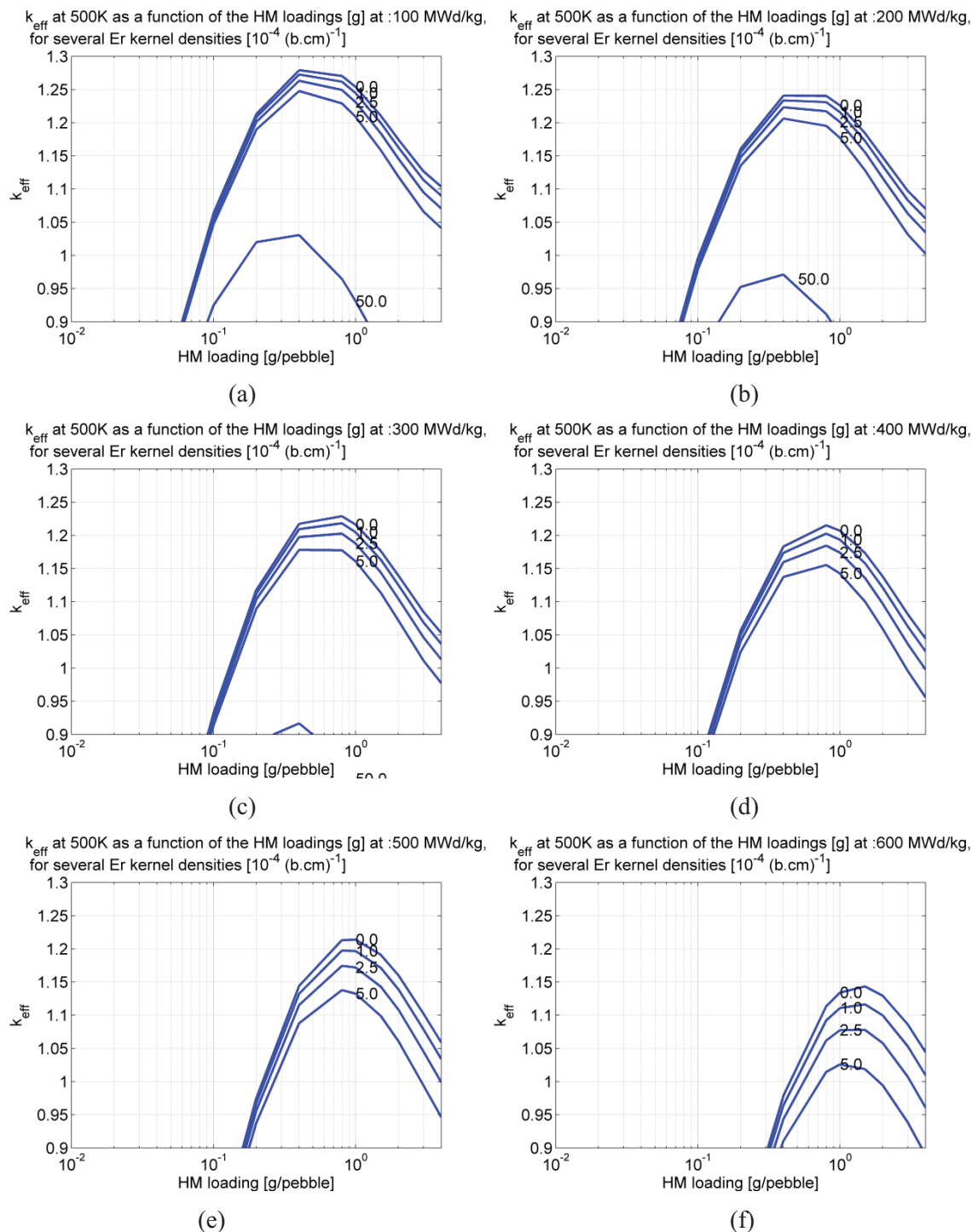
Figure 9. k_{eff} for a radial slab with pebbles having several HM loadings burnup levels and Er-167 concentrations.

3.1.4   Effect of the Location of the Erbium within the Pebble on the Temperature Coefficient

Minimization of the amount of burnable poison in the core is desirable, since its presence reduces the achievable discharge burnup. It would be attractive to have the poison only in the pebbles (pebble core zones) with a high burnup (i.e., in the zones that exhibit a positive temperature reactivity feedback coefficient). To avoid using a high initial Er concentration to ensure a significant amount of Er at high burnup the self shielding of the Er particle in the beginning of the irradiation is increased by increasing its radius.

In this section the self shielding effect of Er-167 is investigated with the radius of the Er-167 particle as a parameter. First, an analytical method for the depletion of the Er-167 particle is adopted using theory for black absorbers [21]. Assuming that the particle is black (i.e., each neutron impinging on the surface of the particle will be absorbed), one can derive the following equation for the Er macroscopic cross section:

$$\Sigma_a(t) = N_p \pi \cdot R_0^2 \left[1 - \frac{\Phi_0}{4NR_0} t \right]^2 \tag{11}$$

in which N_p is the number of poison particles, R_0 the particle radius, $\Phi_0 t$ the neutron fluence, and N the poison nuclide density. Note that for a fixed poison density per pebble the initial macroscopic cross section $\Sigma_a \sim N_p^{1/3}$ and therefore putting all the poison material in a single particle results in the lowest initial cross section. Furthermore, the initial change of the cross section $\frac{d\Sigma_a}{dt} \sim -N_p^{2/3}$, resulted in a slower initial change of the cross section at the beginning of irradiation for cases with a small number of poison particles.

Figure 10 shows the relative macroscopic cross section as a function of time with the number of particles as a parameter. It shows that if we would like to have effective Er-167 self shielding during the beginning of the irradiation (which would result in a slower depletion of the poison) the entire amount of the poison should be put in only several particles. The red crosses in the graph show the point at which the particle is no longer black (i.e., $R < 3\ mfp$). Clearly, the particles are not actually black and therefore a quantitative calculation of the self shielding effect is performed using SCALE-6 calculations in the following part of this section.

Using a fixed (homogeneous) concentration of 2.0×10^{-6} (b.cm)$^{-1}$ the homogenized microscopic cross section of Er-167 is calculated for several cases:

a.   The poison is put in separate particles in the same matrix as the fuel particles.

b.   The poison is mixed homogeneously with the fuel in the same (fuel + poison) particle.

c.   The poison is put at the very center of the fuel particle using the fuel to shield the poison at the beginning of the irradiation. The radius of the Er center part of the kernel is 40 μm.
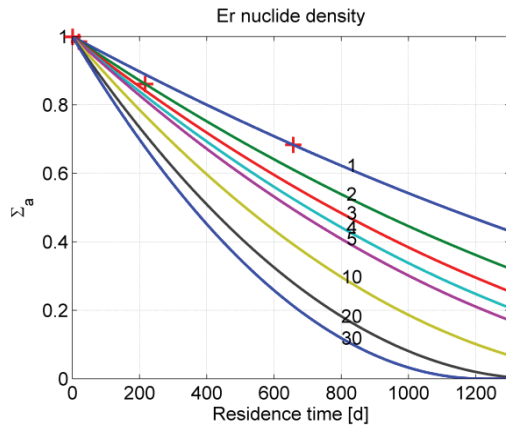
Figure 10. Er-167 macroscopic cross section (relative) as a function of the residence time in the core for several numbers of Erbium particles. The red crosses show the point where the particles can be seen as black absorbers.

The results are presented in Table 4, including the absorption cross sections for Pu-239 and Pu-241. It can be seen that the Er-167 and Pu-239 and 241 indeed shield each other significantly for all cases (a–c). The Er-167 cross section is the lowest for Case c in which it is both significantly shielded by the fuel and itself. The self-shielding seems to be the more important than shielding by the fuel, when one compares Case a to b.

The poison particle size is varied to further investigate the self-shielding effect. The total poison content per pebble is kept at the same fixed amount. The results of this study are presented in Figure 11. One can see that the cross section varies significantly with the number of poison particles per pebble. The size of the poison particles is calculated according to the formula:

$$R_{part} = \sqrt[3]{\frac{\overline{N}_{Er} R_{peb}^3}{N_{Er} n_{Er} \psi}}$$ (12)

Table 4. Er-167, Pu-239, and Pu-240 microscopic (absorption) cross section for several cases: (a) poison in separate particles (48800), (b) homogeneously mixed in the fuel kernel, (c) heterogeneously at the center of the fuel particle; and (d) for the reference case (without Er).

Case	$\sigma_{a,Er\text{-}167}$	$\sigma_{a,Pu\text{-}239}$	$\sigma_{a,Pu\text{-}241}$
a	150 b	76 b	71 b
b	180 b	74 b	70 b
c	143 b	76 b	71 b
d	-	90 b	80 b

Figure 11 confirms what was found with the analytical investigation (Equation 11), namely that putting all the Er in a single particle yields the highest self-shielding. This shielding effect is larger than putting the Er at the center of the fuel kernels.
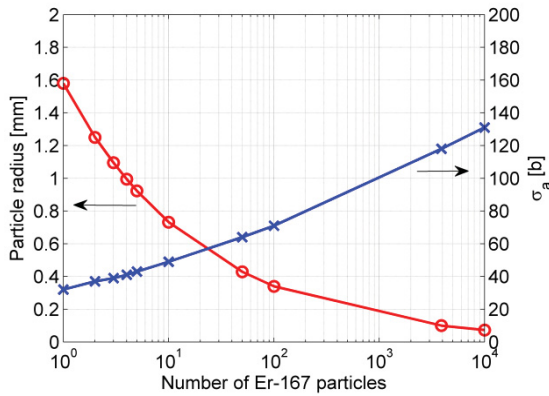
Figure 11. The homogenized Er-167 microscopic (absorption) cross section as a function of the number of poison particles per pebble for a fixed total Er amount (blue line). Poison particle radius for number of Er-167 particles (red line).

3.1.5   Conclusions on the Improvement of the Temperature Coefficient

In practice, the core of a pebble bed reactor is a mix of pebbles with different burnup levels, which results from the recirculation of the pebbles. Normally the zones with the highest burnup value can be found near the (inner) reflector at the bottom of the core, since the pebbles move down with time (burnup) and the highest thermal flux levels in the pebble bed are found near the inner reflector. The PEBBED, THERMIX, and SCALE-6 codes have been used to calculate the average nuclide densities, which represent the mixture of pebbles having different burnup levels, for several core zones. These nuclide densities are used to calculate the temperature coefficients as a function of the axial core position in a procedure similar to the one used in the previous sections. Figure 12 shows the UTC for several axial positions as a function of the temperature. It can be seen that at low temperatures (T < 800 K) a significant portion (75%) of the core has a positive UTC.

(a)   (b)
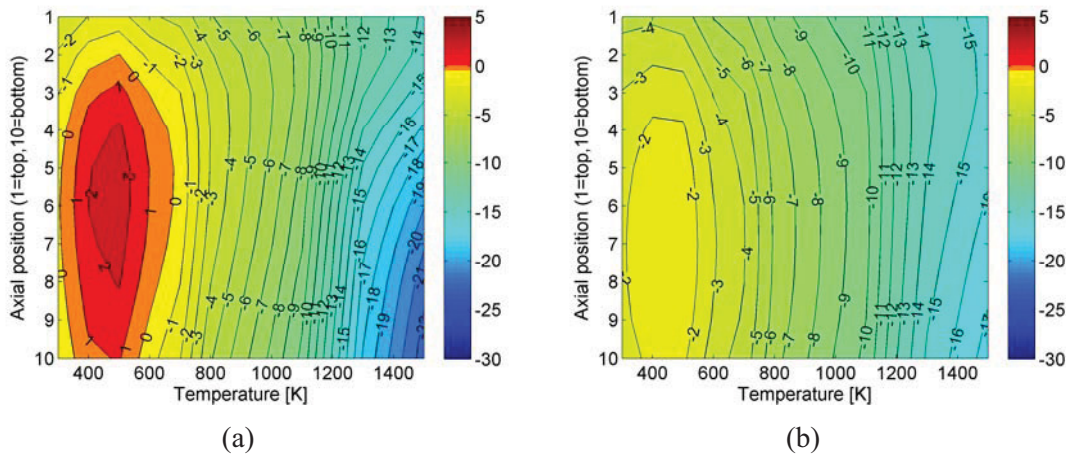
Figure 12. Uniform Temperature Coefficients of reactivity in the Deep-Burn (Pu-fueled) PBMR as a function of the axial core position and the temperature; for the reference case without addition of Er (a) the core has a positive UTC at low temperatures at the bottom region; for a case in which Er-167 was added at a density of 2.0×10^{-6} (b.cm)$^{-1}$ to the fuel kernel (b) a core-wide negative UTC is found for the entire temperature range.

Table 5 shows the key results of the full core parameter study in which the HM loading per pebble was varied between 2 and 3 g per pebble and the Er-167 density in the kernel between 0 and 2.0×10^{-6} (b.cm)$^{-1}$. The first two cases represent the reference core and fuel design for the two DB fuel types (with or without MAs). It is noted that for the reference case with initial MA in the fuel the maximum UTC in the core is lower as compared to the Pu-only fuel. This is the result of the lower discharge burnup in the Pu + MA-fueled core.

For the last three cases presented in the table, a cylindrical core concept (Section 3.2) was adopted with the improved coated particle design of Section 4.4.

It can be seen that by either increasing the HM load or by adding more Erbium the UTC decreases and can be made negative for the entire temperature range. This is in agreement with the simplified cases investigated in the previous sections.

The drawback of increasing the HM load is that the fast fluence attained by the pebbles increases. Experience with TRISO fuel for fast fluence levels above 8×10^{21} n/cm^2 is lacking and is therefore unattractive. A loading of 3 g per pebble without burnable poison would get close to attaining this fluence level. On the other hand, increasing the Er-167concentration reduces the pebble discharge burnup and the Pu destruction capability of the reactor.

The temperature coefficient can be improved by addition of Er-167 and/or increasing the HM load per pebble without significantly sacrificing the pebble discharge burnup. The present analysis suggests that increasing the HM load from 2 to 3 g per pebble without burnable poison addition is the most attractive option with regards to the achievable burnup. This option would keep the discharge burnup at 690 MWd/kg, while keeping the maximum UTC below -1 pcm/K. It is noted, however, that the high fast fluence levels will be attained $\Gamma > 7.0 \ 10^{21}$ cm^{-2} (E > 0.1 MeV) for loadings larger than 2.5–3g per pebble. It is unclear whether material integrity is secured for these flux levels. Furthermore, the higher initial fuel loading per pebble will also result in a higher amount of minor actinides per pebble at the end of the irradiation. This can have an increased decay heat level per pebble as a result.

Table 5. Key results of the optimization of the DB pebble bed core for several HM land Er-167 loadings and fuel types.

Case	Fuel Type	HM Loading [g/pebble]	Er-167 kernel density [(b.cm)$^{-1}$]	Discharge burnup [MWd/kg]	Core maximum temperature [K]	Discharge fluence E > 0.1MeV [10^{21} cm^{-2}]	Core maximum UTC [pcm/K]
1	Pu + MA	2	0	505	1335	3.51	+0.70
2	Pu	2	0	687	1284	4.90	+2.58
3	Pu	2	1.0×10^{-6}	669	1272	4.76	+1.26
4	Pu	2	2.0×10^{-6}	620	1299	4.38	-1.20
5	Pu	2	2.5×10^{-6}	525	1340	3.62	-2.76
6	Pu	3	0	690	1285	7.23	-1.43
7	Pu	3	1.0×10^{-6}	660	1308	6.81	-2.72
8	Pu	3	2.0×10^{-6}	600	1339	6.02	-3.68
9	MAO$_{1.8}$(SiC)$_{0.6}$*	2	0	567	1189	4.45	-0.74
10	MAO$_{1.8}$(SiC)$_{0.6}$	2	0.5×10^{-6}	487	1259	3.79	-2.22
11	MAO$_{1.8}$(SiC)$_{0.6}$	2	0.7×10^{-6}	457	1280	3.56	-2.54

*See Table 12 and Table 13 for fuel type specifications.

One can also choose to add Erbium to the pebbles to improve the temperature coefficient. A penalty of ~100 MWd/kg on the achievable burnup has to be paid to ensure a negative temperature coefficient for the entire core and temperature domain. From the previous sections it was found that the Erbium can possibly made more effective by using separate particles or by locating the Erbium at the very center of the coated fuel particles or as separate particles.

Erbium is depleted as the pebbles move downward in the pebble bed core for the cases with Erbium addition to the fuel. As a result, the power peak shifts downward with increased Erbium loading, since a higher concentration of the (Erbium) absorber material is located at the top of the core. For the reference case (without Erbium) the power peak matches the axial fluid temperature profile, resulting in a relatively flat fuel temperature profile. With the power peak shifted downward, higher fuel temperatures are encountered as can be observed in Table 5. The maximum fuel temperature can probably be reduced for these cases by reducing the total number of pebble (re)circulations. However, this would probably in turn increase the maximum UTC in the core, since the Erbium is less effective at the core bottom region, where it is needed most.

3.2 Reduction of the Power and Temperature Peaking in the Core

This section presents the studies performed that aim at a reduction of the power peaks in the DB pebble bed core, which are present near the inner and outer reflector. A scoping study (in which the geometry and material composition of the core has been varied) has been performed first. This analysis uses a 1-D transport calculation in XSDRNPM, which represents a radial slice of the core and the reflector(s). This study was followed by a full core calculation for the most promising concepts. It is noted that in the scoping studies of Sections 3.2.1–**Error! Reference source not found.** the free-gas approximation for collisions in the thermal energy range of carbon was assumed for graphite. In the following full core analysis of Section 3.2.5 additional $S(\alpha,\beta)$ thermal moderator data for graphite was adopted. No significant differences in the trends were observed between the simplified and the full core studies.

The following parameters were varied in the preliminary scoping study:

1. The outer radius of the pebble bed in a cylindrical core design

2. The outer radius of the inner reflector

3. The graphite density of the inner reflector

4. The number of graphite-only pebbles in the pebble bed

5. Be_2C concentration as moderator material.

The optimal power (thermal flux) profile would be a radial flat one during normal operation resulting in a radially flat temperature distribution. For a depressurized LOFC incident in which the heat is transported by conduction and radiation to the outer surface of the reactor a profile with a peak at the outer rim of the core, it is optimal.

3.2.1 Influence of the Size of the Outer Radius of the Pebble Bed in a Cylindrical Core Design on the Thermal Flux

The most straightforward way of reducing the peak in the thermal flux near the inner reflector is by removing this reflector entirely. The result is a cylindrical pebble bed core with only an outer graphite reflector similar to the HTR-MODULE [22] and HTR-PM designs.

The result of the thermal flux profile is shown in Figure 13. It is almost radially flat except for the region near the outer reflector where the peak remains. Its level is more than four times the value of the flux at the core center. The peaking is not reduced when the pebble-bed radius is reduced in size. The moderating

effect of the reflector on the core neutron spectrum appears to only be felt within a short distance of the reflector.
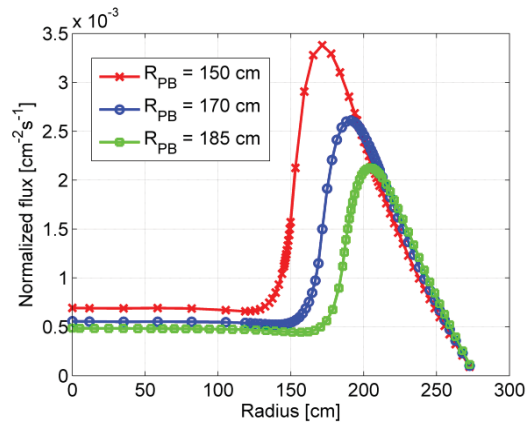
Figure 13. Thermal flux profile (radial) in a cylindrical pebble bed reactor with the pebble bed outer radius as a parameter.

3.2.2   Influence of the Size of the Outer Radius of the Reflector in an Annular Core Design on the Thermal Flux

In a less drastic way, the inner reflector is not entirely removed but reduced in size. Figure 14 shows that one would have to reduce the radius of the inner reflector to a small size (R < 10 cm) to make a significant reduction.
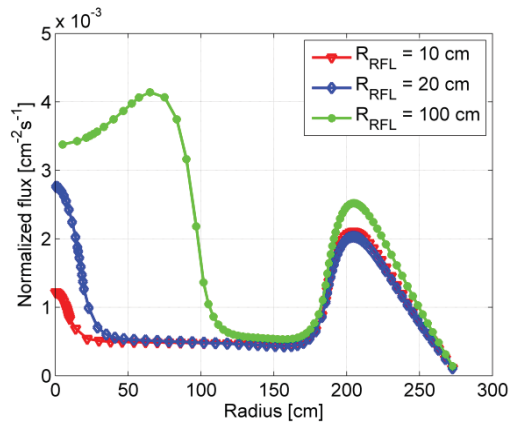
Figure 14. Thermal flux profile (radial) in an annular pebble bed reactor with the radius of the outer reflector as a parameter.

3.2.3   Influence of the Inner Reflector Density in an Annular Core Design on the Thermal Flux

The peak near the inner reflector could also be reduced by reducing the graphite density of the inner reflector. The results are shown in Figure 15. A reduction in the density clearly changes both the shape and the peak value of the thermal flux. The peak shifts to the center of the core, while it increases first and then decreases for low graphite densities.
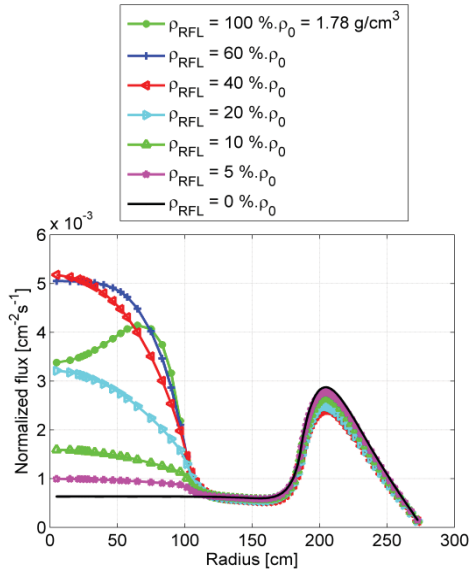
Figure 15. Thermal flux profile (radial) in an annular pebble bed reactor with the density of the inner reflector as a parameter.

3.2.4   Influence of the Ratio of Graphite to Fuel Pebbles in a Cylindrical Core Design

A cylindrical-core geometry is adopted in which the ratio of number of graphite-to-number of fuel pebbles is varied. Figure 16 shows the radial thermal flux profile. The ratio of the peak flux in the reflector (and pebble bed) to the average flux in the pebble bed decreases with increasing numbers of graphite pebbles in the core. For a high number ($n_{gr}/n_{tot} = 70\%$) of graphite pebbles the thermal flux has a larger gradient in the pebble bed.

The profile for $n_{gr}/n_{tot} = 50\%$ has the desired behavior (i.e., a relatively flat profile within the pebble bed) of a relatively small peak at the core outer region as compared to the reference flux profile.
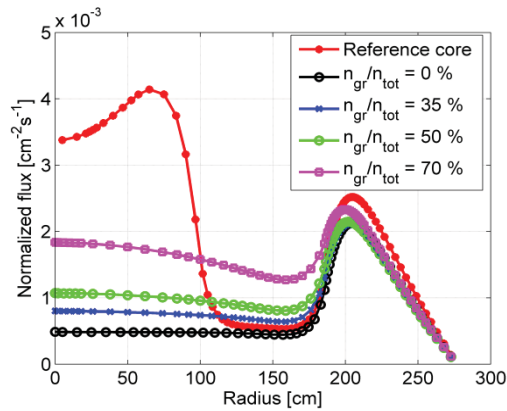
Figure 16. Thermal flux profile (radial) in a cylindrical pebble bed reactor with the number of graphite pebbles to the total (graphite + fuel) number of pebbles as a parameter.

Since the moderator-to-fuel ratio in the core has changed, it is expected that the MTC will deteriorate. One can estimate the effect from Figure 8(a). The case of 50% graphite pebbles in the core is equivalent

to an average fuel loading of 1 g per pebble. Figure 8(a) shows that for this case a positive MTC at 500 K for high burnup levels is to be expected.

3.2.5   Conclusion on the Power Peak Reduction

From the scoping studies presented in the previous sections, two cases were selected and further investigated with a full core analysis with PEBBED-THERMIX-SCALE: a reduced center reflector; and a cylindrical core design. Key results are presented in Table 6.

The effect of the reduced inner reflector graphite density and a cylindrical core design on the power peak is shown in Figure 17 (a) and (b), respectively. It can be seen that for a low graphite density ($\rho = 0.05\rho_0$) the inner peak in the thermal flux completely disappears and that the power peak also vanishes (Figure 15 and Figure 17 [a]). The power peak in the core, which is now located near the outer reflector, is 12.1 MW/m^3. As a result the maximum temperature during an LOFC transient reduces from 2072 K to 1871 K ($\rho = 0.05\rho_0$). Furthermore, the maximum fuel temperature that a given pebble experiences during its lifetime reduces from 1541 K to 1301 K.

As an alternative to the annular core with a transparent inner reflector, a cylindrical core design is adopted in this section in an attempt to avoid power (and temperature) peaking in the inner and outer core region. The proposed design is based on the HTR-PM design (Figure 18 [a]), which has a pebble bed core diameter of 3 m, a height of 11 m, and a thermal power of 250 MW. As compared to the PBMR-400 design, the helium coolant inlet and outlet temperature have been lowered to 250°C and 750°C, respectively, and the number of pebble passes is increased from 6 to 20. For further details of the design and material properties see Zheng et al.'s article [23].

(a)   (b)
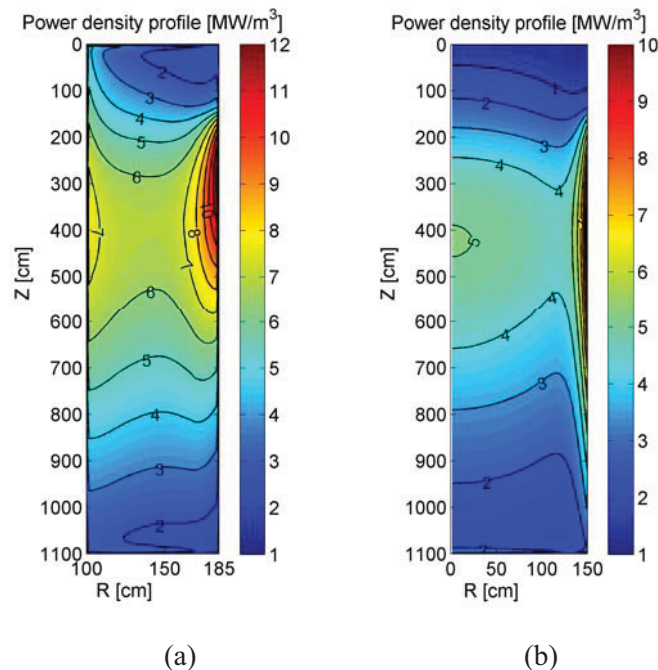
Figure 17. (a) Power density profile of an annular core with reduced inner reflector density ($\rho = 0.05\rho_0$) and (b) the profile in the DB HTR-PM (cylindrical) design with 20 pebble circulations.

(a)   (b)
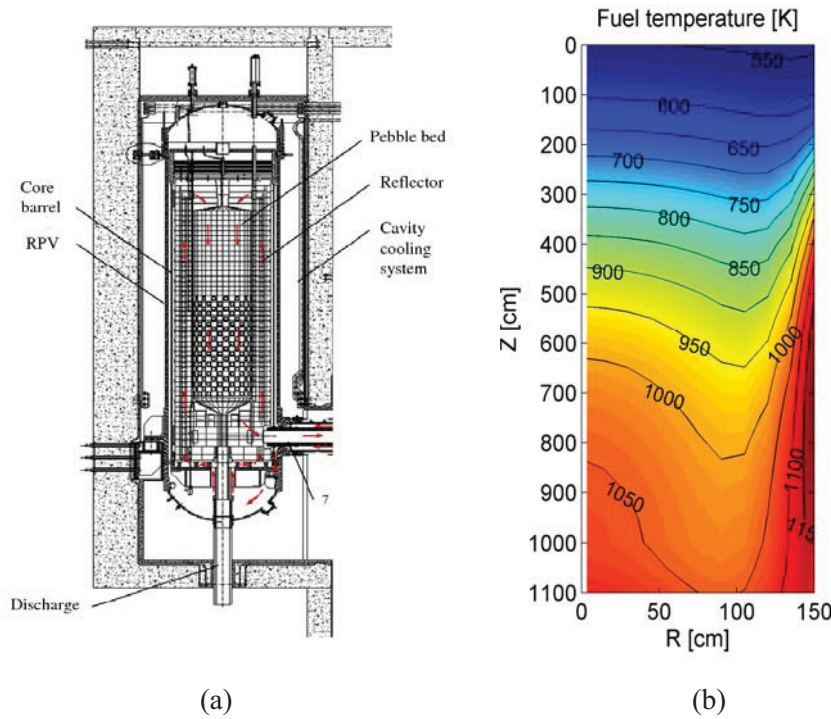
Figure 18. (a) The 250 MW$_{th}$ cylindrical HTR-PM design and (b) the temperature profile (pebble center) for a DB fuel loaded core.

(a)   (b)
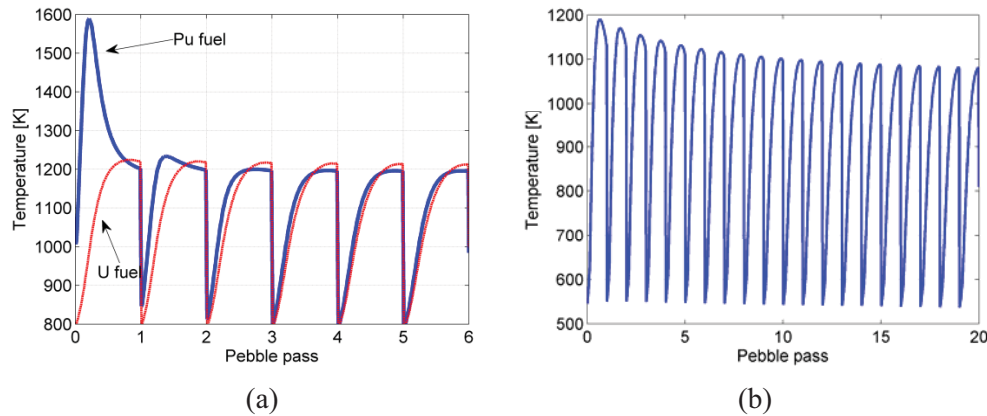
Figure 19. (a) The temperature history of a pebble in the PBMR-400 for both UO$_2$ fuel and Deep-Burn fuel (6 pebble circulations); and (b) the temperature history in the DB fueled HTR-PM design (20 pebble circulations).

The power density profile of the DB HTR-PM design is shown in Figure 17(b). It can be seen that the power profile is flattened in the radial direction as compared to the power profile of the annular core (Table 6), while a higher discharge burnup of 567 MWd/kg is achieved. The power peak at the core center, where the maximum temperature occurs, is reduced from 17.7 MW/m^3 to 10.8 MW/m^3. The power profile is flattened in the axial direction as a result of the increased pebble in-core (re)circulation (increased from 6 to 20).

As compared to the reference design the core maximum temperature at nominal conditions is reduced from 1335 K to 1189 K (Figure 18). The maximum fuel temperature during the first pebble pass is

reduced from 1406 K to 1190 K (Figure 19), and the maximum fuel temperature during a DLOFC transient is reduced from 1961 K to 1734 K. It is noted that these temperatures are calculated using a conservative graphite thermal conductivity, which is fixed at a value of 26 W/m/K. The maximum temperature in a cylindrical design during an LOFC, which is also know as a conduction cool-down event, is sensitive to this conductivity. If a temperature dependent (best-estimate) conductivity based on German data [23] is used, the temperature peak is expected to be 50 K lower (Section 3.4).

Table 6. Key results of the optimization of the DB pebble bed core with respect to the maximum power and temperature for several HM core and fuel types.

Case	Fuel Type	Core Type	Norm. Reflector Density	Discharge Burnup [MWd/kg]	T core max. [K]	T Pebble Peak [K]	q''' core [MW/m^3]	q Pebble Peak [kW]	T DLOFC max. [K]
1	Pu+MA	Annular	1.0	505	1335	1406	20.8	3.07	1961
2	Pu	Annular	1.0	687	1284	1541	17.7	6.03	2072
3	Pu	Annular	0.05	700	1272	1301	12.1	4.28	1871
4	Pu	Annular	0.10	699	1299	1311	11.8	4.72	1910
5	Pu	Annular	0.20	699	1340	1493	13.8	7.23	2101
6	$MAO_{1.8}$ $(SiC)_{0.6}$*	Cylinder	N/A	567	1189	1190	10.8	2.35	1734

*See Table 12 and Table 13 for fuel type specifications.

3.3 Analysis of the Decay Heat of Deep-Burn Fuel

The decay heat of DB fuel is expected to be different in magnitude than that of 'standard' UO_2 fuel. The decay of fission products and unstable minor actinides is mainly responsible for the decay heat in used fuel. The spectrum of fission products is expected to be slightly different in DB fuel compared to UO_2 fuel. Furthermore, DB fuel consists of Pu with possible addition of minor actinides. This reduces the time path from initial fuel to the production of unstable minor actinides. Their contribution to the decay heat can therefore be considerable in DB fuel.

3.3.1 Method for Calculation of the Decay Heat

A procedure for the calculation of the decay of different (pebble) fuel types at several burnup levels was made using SCALE-6. It consists of the modules CSAS and ORIGEN-S, which are controlled by an in-house Perl script.

The procedure is as follows:

1. Problem-dependent cross sections for the pebble fuel are generated using CSAS. The 'doublehet' option is used and microscopic-weighted cross sections are created.

2. The COUPLE code automatically couples the problem-dependent cross section constants and flux weighting factors into libraries used by ORIGEN-S for performing calculations of isotopic depletion and generation and their associated decay heat.

3. A depletion step is performed in ORIGEN-S using a fixed power per pebble and a chosen time interval. In this way the burnup level after each depletion step is exactly know ($B = \overline{P} \cdot \Delta t$).

4. Steps 1 through 3 are repeated to update the microscopic cross sections and perform the depletion calculation of the next time interval.

5. The decay heat curve at each burnup level is calculated. First, the fuel is irradiated with a fixed flux level (a typical HTR one energy group flux level of 1×10^{14} cm-2s-1). This step is performed to re-normalize the short-lived nuclide concentrations to the same level for each burnup level of the fuel. Note that these burnup levels were attained by using a fixed power level, which leads to a variable flux throughout the depletion calculations.

The contributions to the decay heat from both the minor actinides and the fission products are calculated. The following sections give the decay heat for Pu only and Pu and MA fuel.

3.3.2   Decay Heat Curves of Pu Fuel

Figure 20 shows the decay heat of Pu fuel for several levels of burnup. It can be seen that the contribution of the actinides to the decay heat is large for the high burnup levels (B > 600 MWd/kg). Furthermore, the decay heat curve from the actinides is different from that of the UO_2 fuel. The MA contribution to the decay heat in the latter fuel types is almost completely determined by U-239 and Np-239, which have half lives of 24 minutes and 2.4 days respectively. Therefore, their decay heat contribution reduces fairly quickly (especially U-239). The latter drop-off is not observed for the Pu fuel and can therefore lead to a large contribution of the actinides to the decay for high burnup levels (Figure 21).

3.3.3   Decay Heat Curves for Pu and Minor Actinide Fuel

Figure 22 and Figure 23 show the decay heat curves of the Pu + MA fuel. The curves are very similar to the Pu-only fuel with a slightly higher contribution of the MA at high burnup levels.

It is noted that the achievable discharge burnup of Pu + MA fuel (550–600 MWd/kg) is generally lower than that of Pu only fuel (675–725 MWd/kg).

The minor actinides that contribute the most to the decay heat of the DB fuel at high burnup are: Cm-242, Am-244, Np-238, Cm-244, and Pu-243. It is noted that the Cm isotopes with respective half lives of 163 days and 18 years generate decay heat for a long period of time.
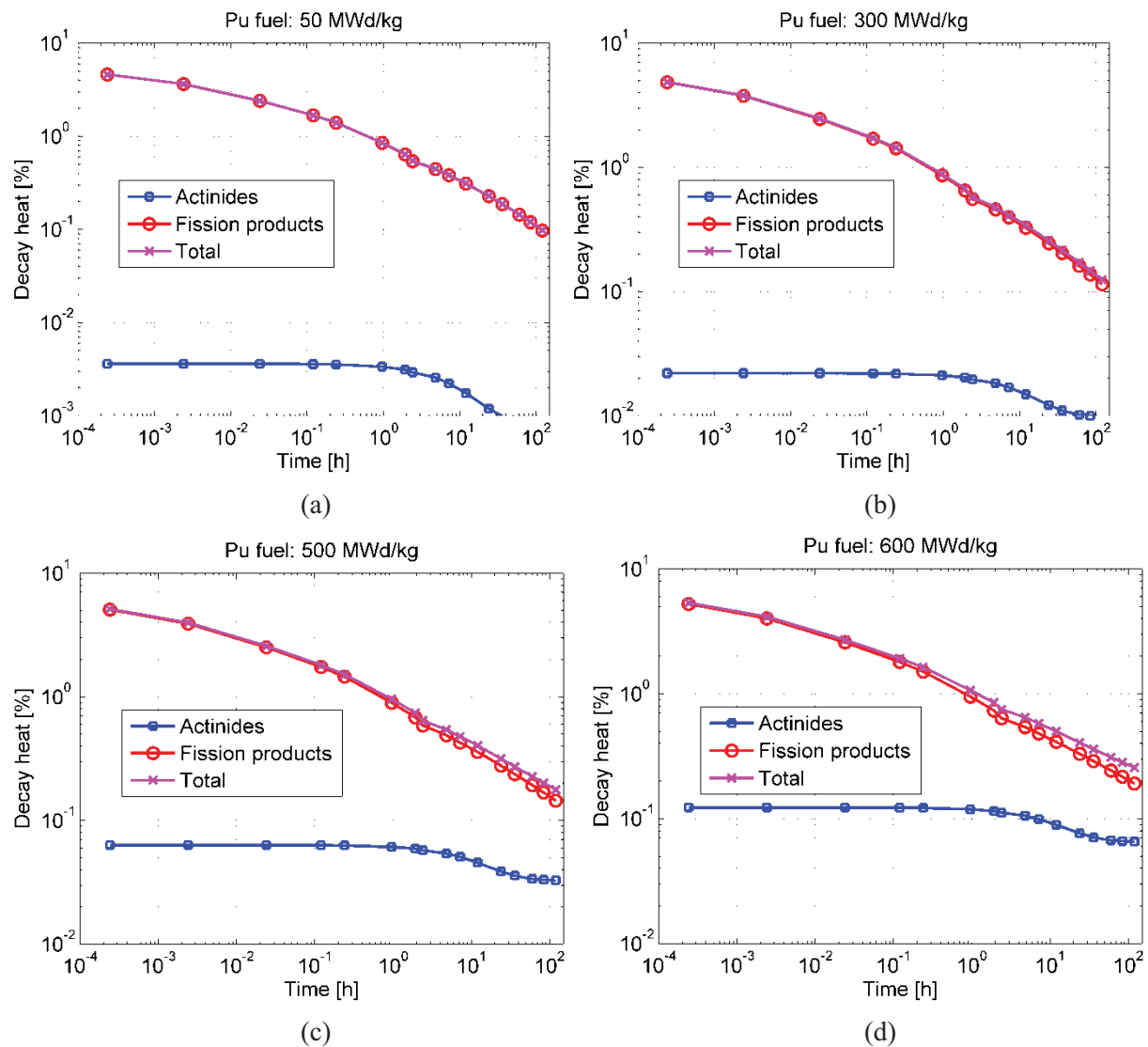
Figure 20. The decay heat from actinides and fission products for several burnup levels of the Pu fuel ([a] 50 MWd/kg, [b] 300 MWd/kg, [c] 500 MWd/kg; and [d] 600 MWd/kg).

(a)   (b)
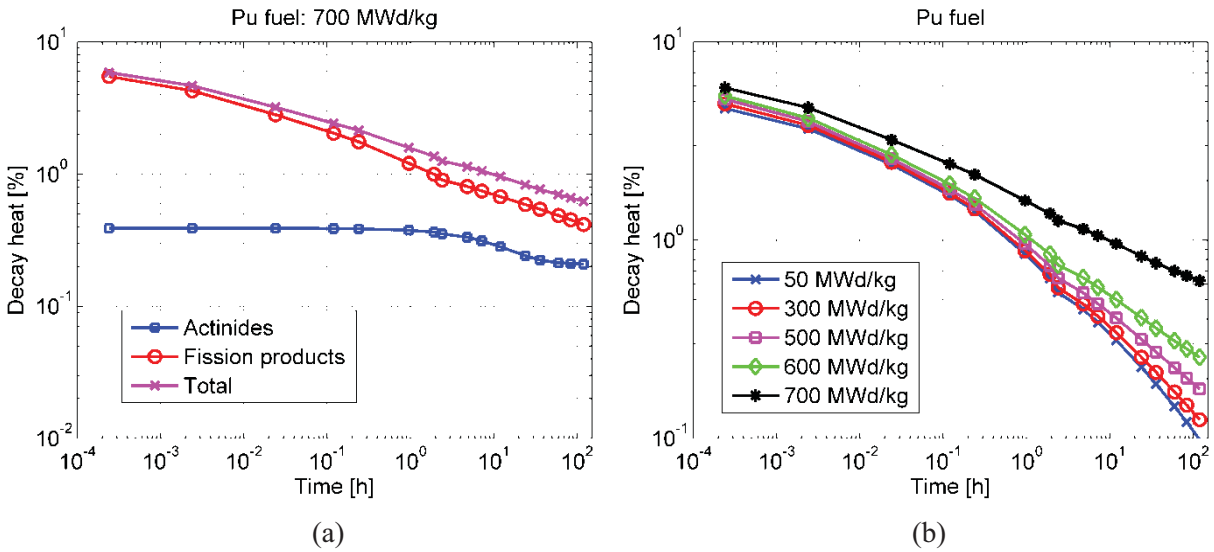
Figure 21. (a) The decay heat from actinides and fission products of the Pu fuel at a burnup level of 700 MWd/kg. (b) Comparison of decay heat curves for Pu fuel at several burnup levels.

(a)   (b)
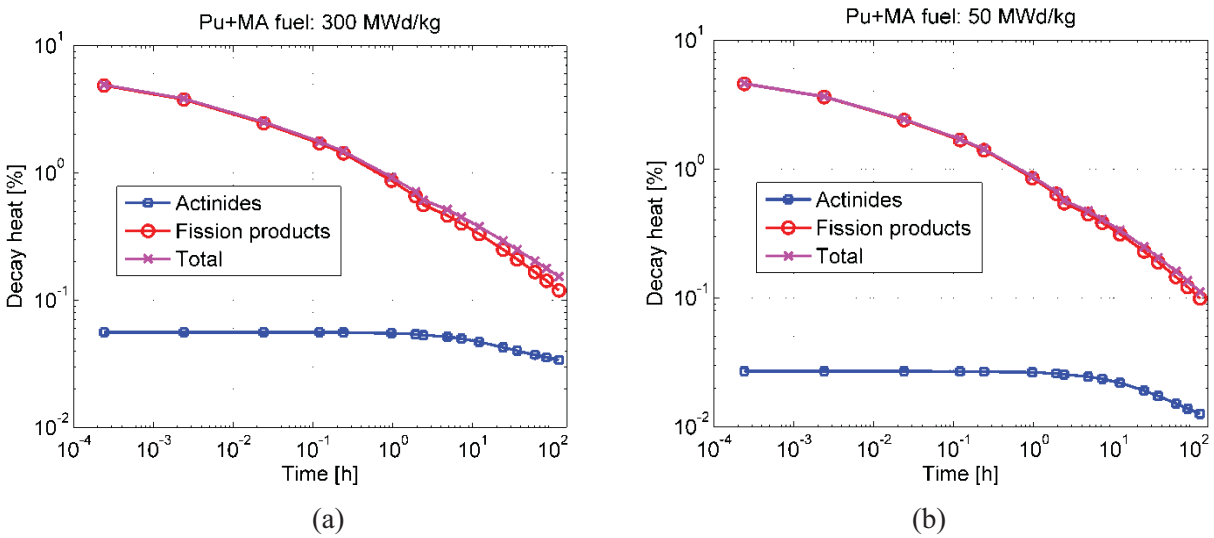
Figure 22. The decay heat from actinides and fission products of the Pu+MA fuel at a burnup levels of (a) 300 MWd/kg, and (b) 50 MWd/kg.
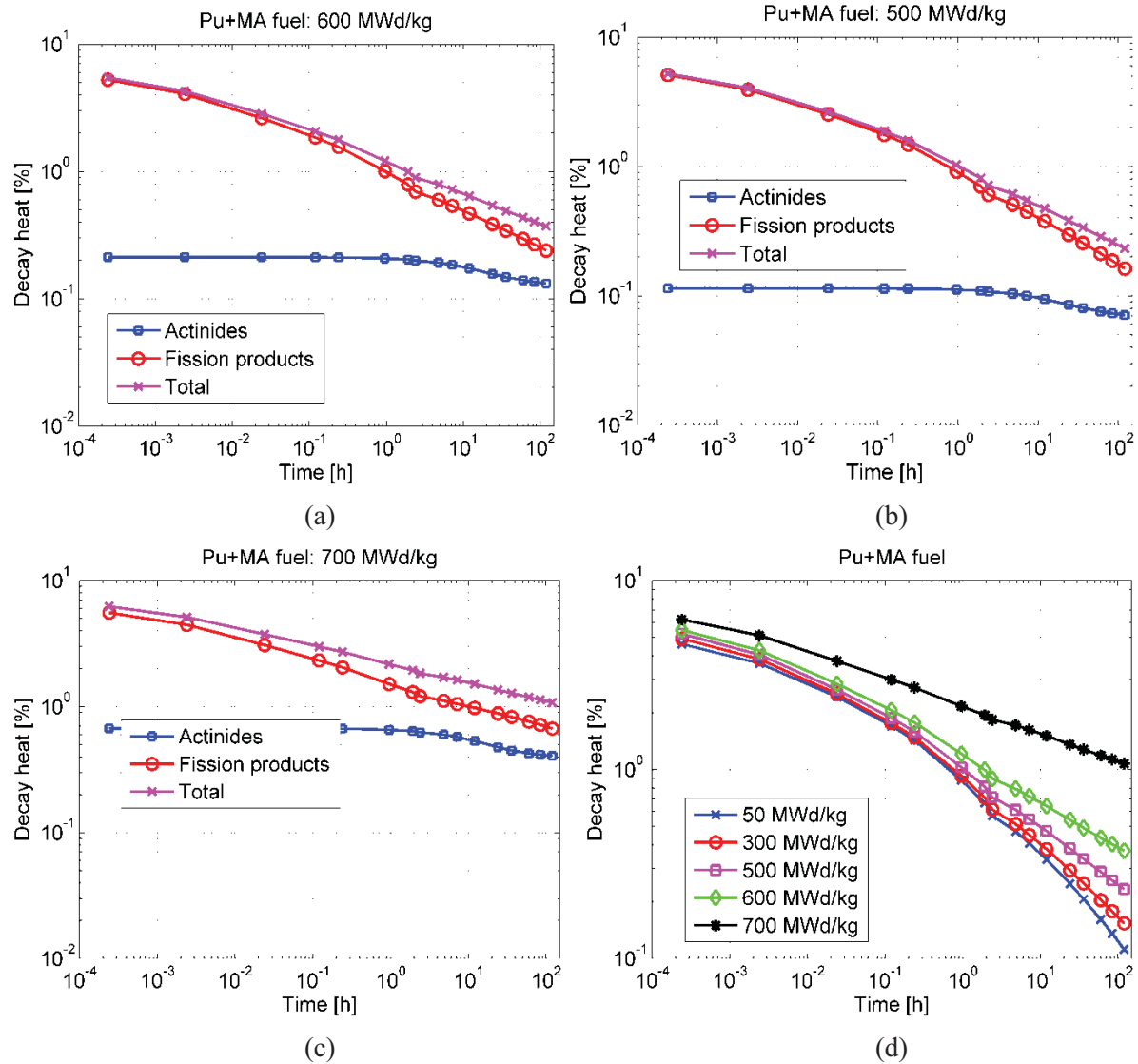
Figure 23. The decay heat from actinides and fission products of the Pu+MA fuel at burnup levels of (a) 600 MWd/kg, (b) 500 MWd/kg, and (c) 700 MWd/kg. (d) Comparison of decay heat curves for Pu+MA fuel at several burnup levels.

3.3.4   Comparison of Decay Heat Curves of UO_2, Pu and Pu+MA Fuels

The decay heat curves of the different fuel types are compared with each other in Figure 24 through Figure 26. From Figure 24 it can be seen that the decay of Pu fuel is lower for the average burnup fuel, but higher for the discharge burnup level fuel when compared with UO_2. This is also true for the case when Pu + MA is compared with UO_2 (Figure 25). The decay heat of Pu + MA fuel at discharge level is however considerably lower than that of the Pu fuel (see Figure 26). This is the result of the lower discharge burnup level of the Pu + MA fuel (600 MWd/kg compared to 700 MWd/kg of the Pu + MA).
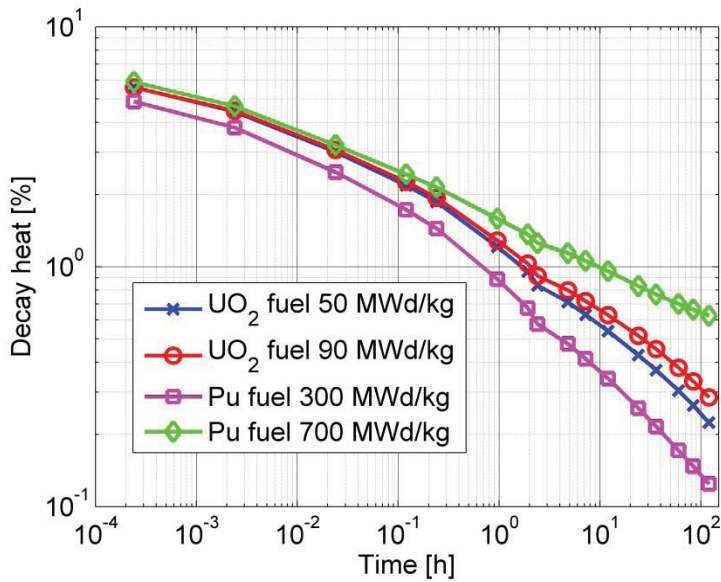
Figure 24. Comparison of the decay heat of UO$_2$ and Pu fuel at the an average burnup (50 MWd/kg for UO$_2$, 300 MWd/kg for Pu fuel) and the discharge burnup (90 MWd/kg for UO$_2$, 700 MWd/kg for Pu fuel).
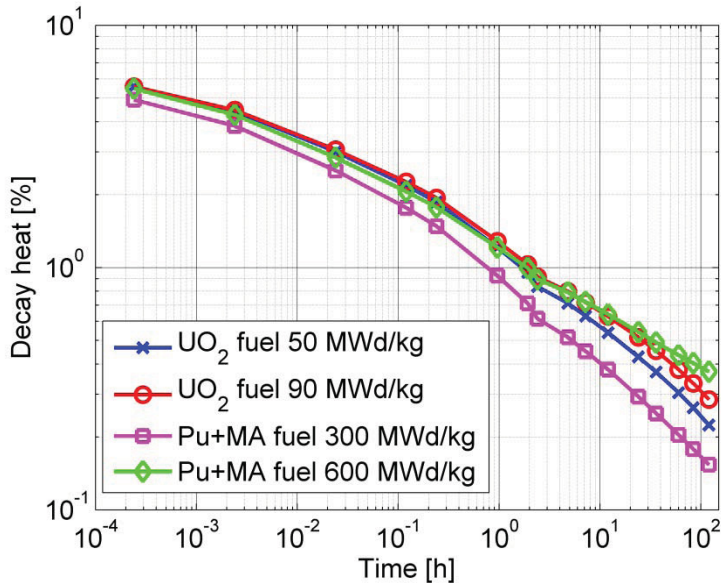
Figure 25. Comparison of the decay heat of UO$_2$ and Pu + MA fuel at the average burnup (50 MWd/kg for UO$_2$, 300 MWd/kg for Pu fuel) and the discharge burnup (90 MWd/kg for UO$_2$, 600 MWd/kg for Pu+MA fuel).
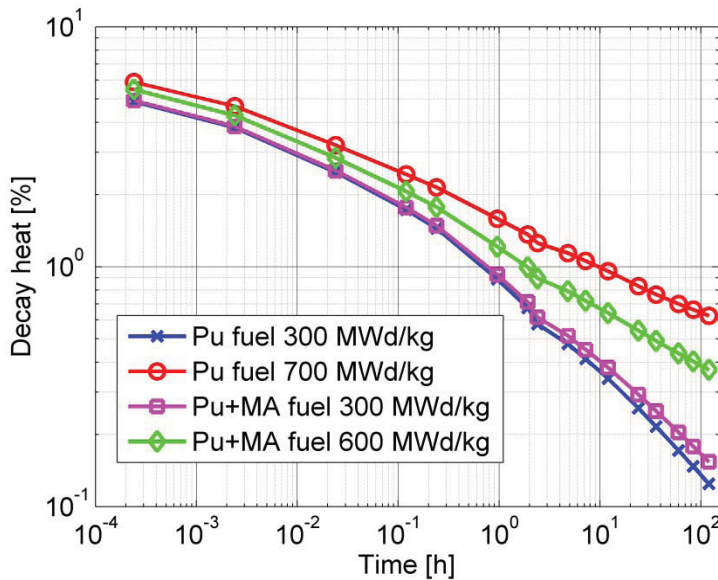
Figure 26. Comparison of the decay heat of Pu and Pu+MA fuel at the average burnup (300 MWd/kg for Pu fuel) and the discharge burnup (700 MWd/kg for Pu, 600 MWd/kg for Pu+MA fuel).

The following conclusions can be made:

1. The decay heat curve of DB fuel is similar to that of standard UO_2 fuel in for low burnup levels.

2. The decay heat curve of the DB fuel at high burnup levels B > 600 MWd/kg is significantly influenced by the contribution of the unstable MAs. These nuclides give a relatively large contribution for these burnup levels, especially after several hours of decay (t > 2 hours).

3. The decay heat curves of the two DB fuels considered are very similar. Because the Pu only fuel is able to attain a higher discharge burnup level, the decay heat is also higher for this fuel type.

3.4   Analysis of the DB HTR-PM under DLOFC Transient Conditions

From the previous section, it was found that the decay heat of DB fuel shows that a significantly higher decay heat level is to be expected for high burnup levels after several hours of decay, when compared to standard UO_2 fuel.

Furthermore, the fast fluence level attained in the DB pebbles is expected to be twice as high as in UO_2 fuel ($\Gamma > 6 \times 1021$ [E > 0.1 MeV]), which could result in a significant reduction in the thermal conductivity of the graphite and the effective conductivity of the pebble bed.

Both effects described above can result in higher (fuel) temperatures during a (depressurized) LOFC incident. The impact of the above effects has been investigated for the Chinese cylindrical HTR-PM design [24]. It was expected that this design provides sufficient margin in the temperature limits for the fuel and metal structures, based on the analysis of Zheng et al. [23].

A model of the HTR-PM has been made in PEBBED-THERMIX and the equilibrium core has been calculated.

3.4.1   Thermal Properties of Graphite

For the thermal conductivity and heat capacity of the graphite material in the core data are used from German measurements that have been incorporated in THERMIX [25].

The following correlation for the graphite matrix conductivity, which is a function of the temperature and the fast neutron dose, has been used in the model:

$$\lambda_{gr,mat} = 1.2768 \left(\frac{-3.906 \times 10^{-5}\,T + 0.06829}{DOSIS + 1.931 \times 10^{-4}\,T + 0.105} + 1.228 \times 10^{-4}\,T + 0.042 \right)$$

(13)

for $450ºC < T < 1300ºC$, $0 < DOSIS < 2.5 \times 10^{21}$ n/cm^2 EDN.

The multiplication factor of 1.14, proposed by Schönfeld, is implemented in this correlation. Note that a neutron fluence level of 1 n/cm^2 EDN $\approx$ 1.76 n/cm^2 E > 0.1 MeV.

For the graphite reflector material surrounding the pebble bed the following correlation is used:

$$\lambda_{gr,refl} = 1.15 \cdot \left[1 + 1.5648 - 0.316 \ln(T + 100) \right] \cdot F$$

(14)

with

$$F = F_1/(Y - F_2) + F_3$$

(15)

$$X = T/1000$$

(16)

$$Y = DOSIS/10$$

(17)

$$F_1 = -0.54705 \times 10^{-2} + 0.38214 \times 10^{-3}\,X + 0.13487\,X^2$$

(18)

$$F_2 = -0.13951 \times 10^{-1} + 0.12064\,X - 0.32955\,X^2$$

(19)

$$F_3 = -0.7264 \times 10^{-1} + 0.41459\,X + 0.23149\,X^2$$

(20)

Equation (2) is valid up to 2000°C, while for the Factor F (Equations [3]–[8]) the temperature and fast neutron dose are limited as follows: $300°C < T < 800°C$, $0 < DOSIS < 30 \times 10^{21}$ n/cm^2 EDN.

The conductivity as a function of the neutron dose is shown in Figure 27(a) for the graphite matrix and in Figure 27(b) for the graphite reflector for several temperatures according to Equations (13) and (14), respectively. It can be seen that for both types of graphite, the conductivity reduces with increasing dose. Furthermore, the conductivity approaches an asymptotic value for high dose levels. It can therefore be expected that the conductivity of the pebbles, the pebble bed and the reflectors is lower in the DB core in general resulting from the higher average fast neutron dose level of the graphite materials. However, the difference in graphite conductivity between a normal and a DB core can be expected to be small, since the conductivity reaches an asymptotic value for dose levels beyond several EDN $\times 10^{21}$.
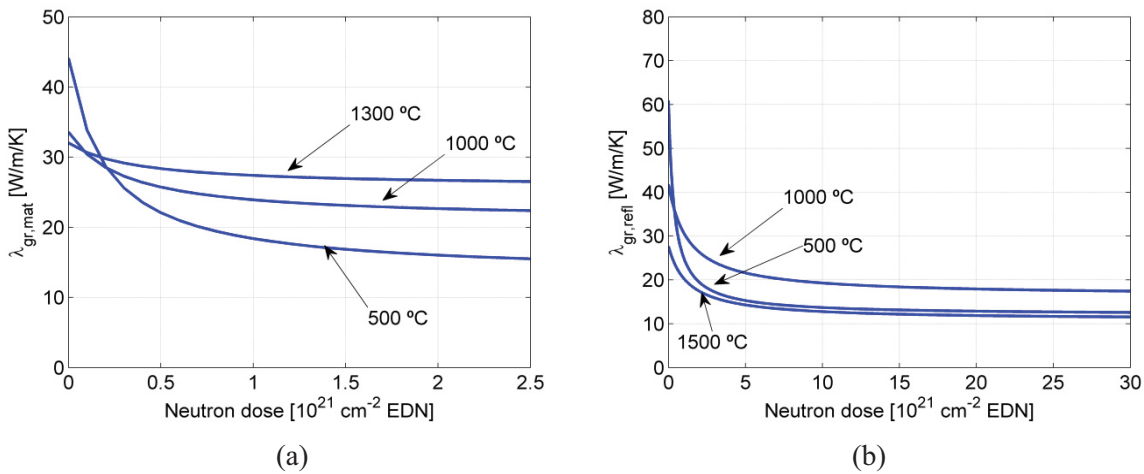
Figure 27. (a) Conductivity of graphite (matrix) in the pebbles according to Equation (13).
(b) Conductivity of graphite reflector material according to Equation (14).

3.4.2   Results of the HTR-PM Core under Normal Operation

The equilibrium core composition has been calculated with PEBBED for the DB HTR-PM and the power density profile (Figure 28a) was determined (Pu-fueled core with 15 pebble [re]circulations). The profile power is similar to the one for the UO_2 fueled core [23] with two power peaks at the core center and outer rim at an axial height of $Z = 300$ cm. The maximum power at the core center is 8.1 MW/m^3, which is higher than for the UO_2 fueled core (6.6 MW/m^3). The resulting temperatures of the solid structures in the reactor are shown in Figure 28(b) and the pebble center temperatures in the core are shown in Figure 29. The highest temperatures occur at the core radial center in the bottom region as a result of the center power peak and the downward flow. The maximum pebble center temperature (860°C) is located at $Z = 675$ cm, while the UO_2 core has a maximum value of 890°C [23]. The average fuel temperature is 600°C for the DB and the UO_2 cores.

(a)

(b)
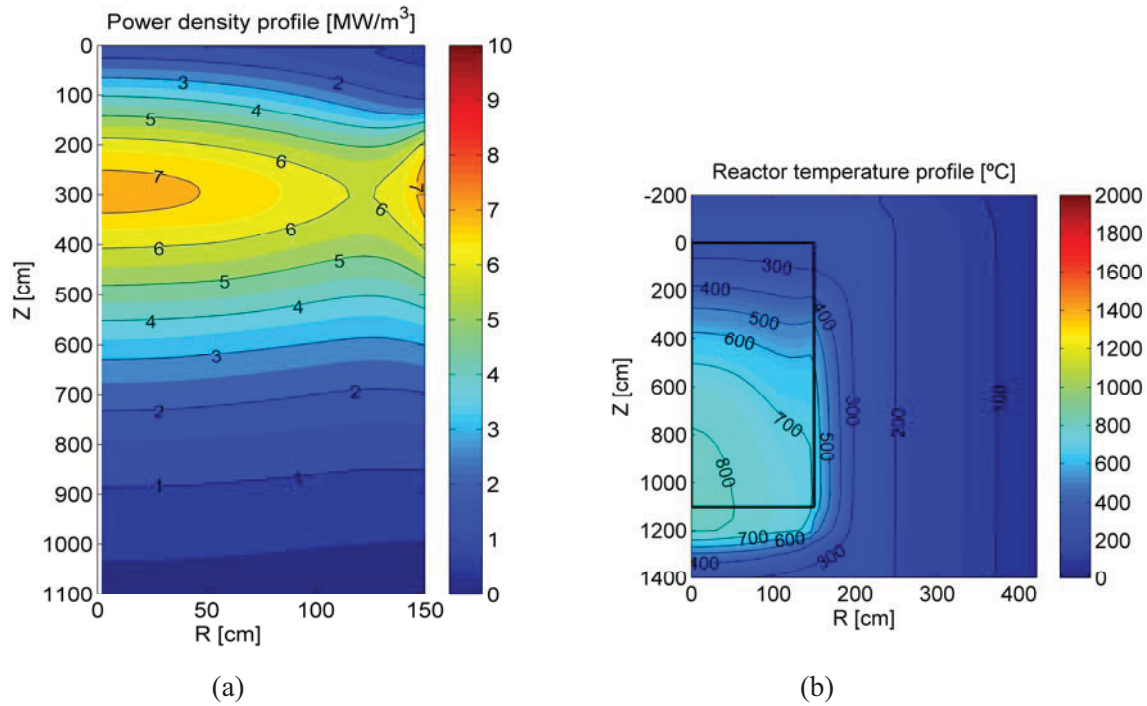
Figure 28. (a) Power density profile in the DB pebble bed core (Pu fuel, 15 pebble circulations); and (b) the temperature profile for the entire DB HTR-PM reactor.
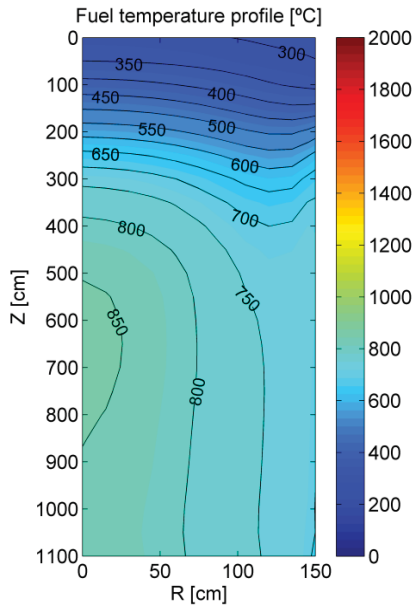
Figure 29. Profile of the pebble center temperatures in the core at the start of the transient. The maximum pebble center temperature in the core is 860°C.

The peak temperatures of the reactor pressure vessel (RPV) and the core barrel (CB) during normal were found to be 150°C and 179°C, respectively. These temperatures are significantly below the value of 250°C for both the RPV and the CB found for in Zheng et al.'s article [23]. This reference considers the

part of the RPV and the CB, where the helium coolant enters the core a temperature of 250°C. This part is not modeled explicitly in the INL model.

3.4.3   Results of the Core during a DLOFC and Code-to-code Comparison

A transient calculation using THERMIX has been performed. It is assumed that the reactor depressurizes instantaneously from 7 MPa to 0.1 MPa and that the coolant mass flow is reduced to zero at the same time. Assuming a reactor SCRAM, the power is determined by the decay only. The standard decay heat curve that is supplied by THERMIX (Figure 30) is assumed first and results are compared with the results in Zheng et al.'s article [23]. A specific decay heat curve for DB fuel is implemented in THERMIX and the impact on the core temperatures is evaluated. Furthermore, the influence of the higher fast neutron dose level of the DB pebbles on the temperature is evaluated.

After the initiation of the transient, the core starts to heat up by the deposition of the decay heat in the absence of forced cooling. Figure 31(a) shows the average and peak fuel temperature in the core during the transient. Heat from the core is transferred to the reactor heat removal system (RHRS) that is surrounding the RPV at a distance of 1 m. These water panels are assumed to be at a constant temperature of 70°C. Heat from the pebble bed core is transferred by conduction and thermal radiation to the side reflector. Heat is conducted through the reflector and the RPV, where thermal radiation effectively transfers the heat to the RHRS. The temperature histories of the RPV and CB are shown in Figure 32(a) and the heat load of the RHRS is given in Figure 32(b).
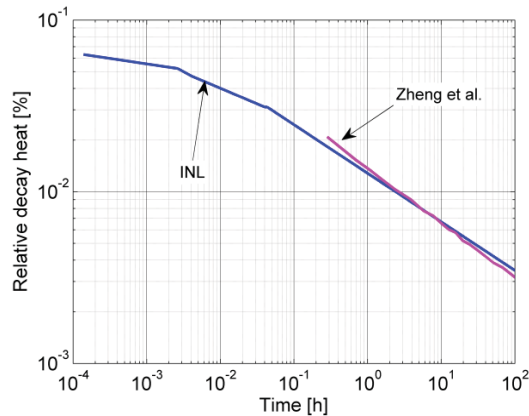
Figure 30. Decay heat curves used in the INL model and in Zheng et al [23].
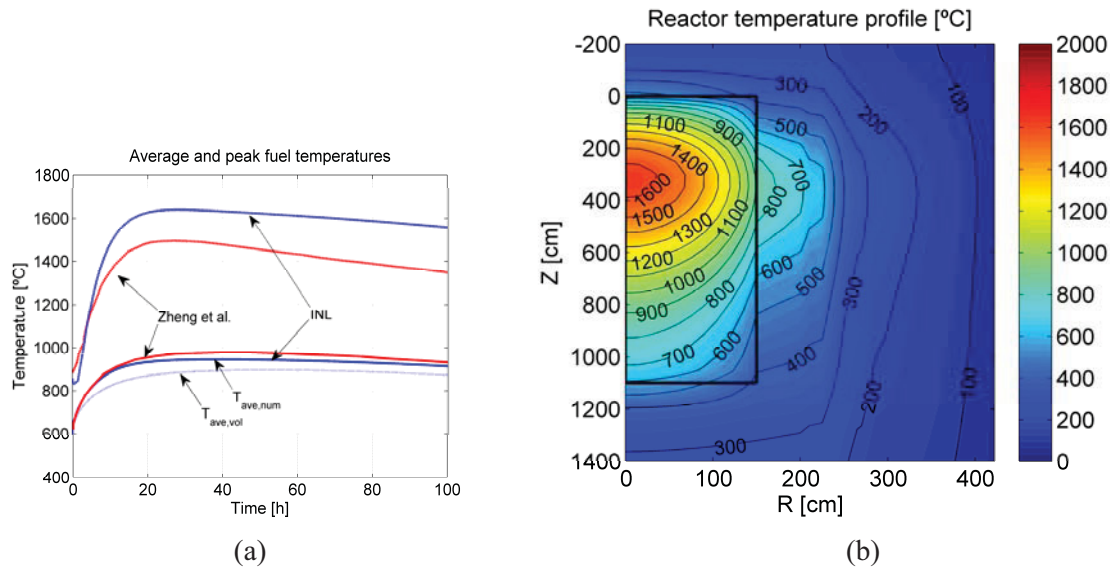
Figure 31. (a) Maximum (dashed line) and average (solid line) fuel temperature during the DLOFC transient for both INL and Zheng et al. results; and (b) the temperature profile for the entire DB HTR-PM reactor at the time point of the maximum fuel temperature.

After the initial heat-up, the core starts to cool down at the point where the decay heat equals the amount of heat transferred to the RHRS. After 27.5 hours, the core reaches a maximum core peak temperature of 1639°C. Figure 31(b) shows the temperature profile in the reactor. The figure shows that only a small part of the core is at this high temperature. This is also reflected in the volume weighted average core temperature, which reaches a maximum value of only 897°C after 52.6 hours.

The results by Zheng et al. [23] for the UO_2 fueled HTR-PM have been shown in Figure 30 through Figure 32. Although the trends are similar, some differences can be identified. The maximum fuel temperature in the core is significantly higher in the INL analysis. It can be seen that the decay heat (Figure 30), the history of the average fuel temperature (Figure 31a) and the heat transferred from the reactor (Figure 32b) compare reasonably well. Therefore, the difference in peak fuel temperature is believed to be caused by the difference in the power profile, which is relatively flat for the UO_2 case [23] compared to the DB case.

Figure 33 shows the radial temperature profile at the (axial) center of the core at t = 50 hours. The temperature profiles of the two results compare reasonably well except for the part close to the core center. From Zheng et al.'s article [23] it was found that the power density during normal operation at this position (Z=550 cm, R=0 cm) is around 4.5 MW/m³, while the calculated power density of the DB core at this position is around 4.0 MW/m³ (Figure 28a). This explains the lower temperature at this position in the DB core and indicates that the higher power peak (8.1 MW/m³ compared to 6.6 MW/m³) at Z=300 cm is responsible for the higher peak temperature at that position.

Furthermore, it was found that THERMIX(-KONVEK) did not adopt Equation (14) in the calculation of the effective conductivity (Zehner-Schlünder) of the pebble bed, but used this equation only to calculate the temperatures within the pebbles. If the code is modified to use Equation (14) in the Zehner-Schlünder equation a reduction of the maximum fuel temperature to 1585°C is found.
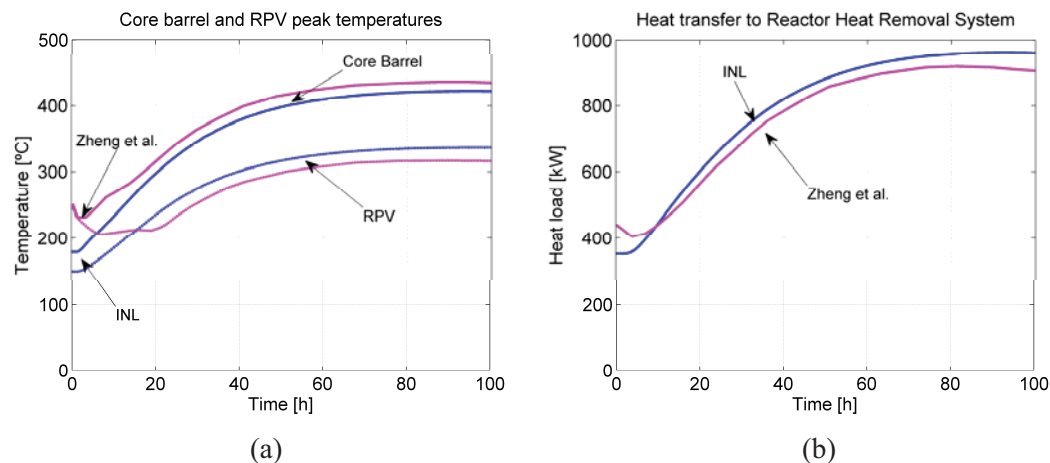
Figure 32. (a) The peak temperature of the RPV and the CB during the DLOFC transient for both INL and Zheng et al. results; and (b) the heat load of the Reactor Heat Removal System.
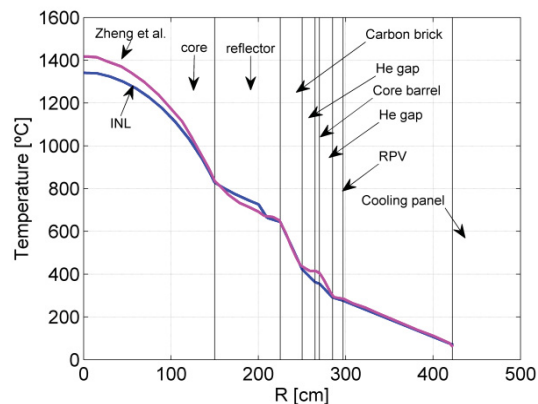
Figure 33. The radial temperature profile at the axial core center during the DLOFC transient at t=50 hours for both INL and Zheng et al.

3.4.4   Impact of the Deep-Burn Decay Heat on the Core Temperatures

The impact of the decay heat curve on the maximum fuel temperature is investigated. A decay heat curve for DB fuel has been calculated with ORIGEN-S and has been implemented in THERMIX. Figure 34 shows the two different decay heat curves and Figure 35 shows the effect on the fuel temperature during the DLOFC transient. The DB decay heat is lower in the beginning of the transient, but higher for t > 5 hours. Therefore, both the average and peak fuel temperature are lower in the beginning of the transient for the case with the DB decay heat. The maximum temperatures are higher and are reached at a later time point in the transient (peak temperature of 1675°C at t = 69.4 hours). While the peak temperature reached is 90°C higher for the DB fuel than for the UO$_2$ decay heat curve, the core peak temperature is lower for the first 16 hours of the transient.
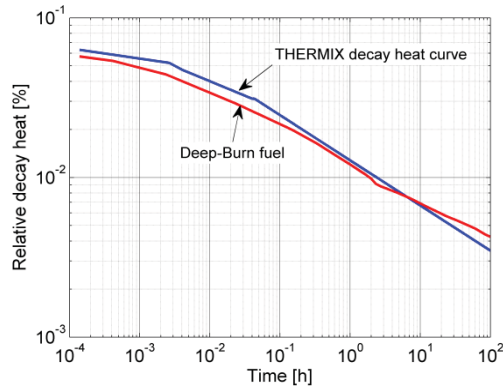
Figure 34. Decay heat curve in THERMIX and a decay heat curve calculated with ORIGEN-S for typical Deep-Burn fuel.
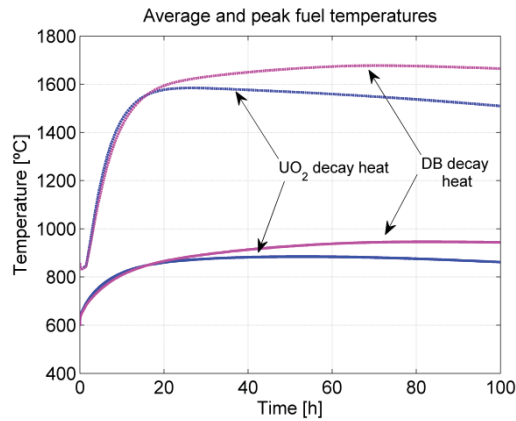
Figure 35. The effect of the different decay heat curves (for UO$_2$ or Deep-Burn fuel) on the fuel average and peak temperatures during a DLOFC transient.

3.4.5   Impact of the Increased Neutron Dose Level on the Core Temperatures

The impact of the neutron dose on the maximum and average fuel temperature, the maximum CB and the maximum RPV temperature during the DLOFC transient has been investigated. Both the fast neutron dose levels of the pebbles and of the reflectors have been varied. Results are presented in Table 7. The maximum values of the peak and average core temperature increase significantly with increasing fast neutron dose level. Both the increase in the dose level of the pebbles as well as that of the reflector have a large effect on the fuel temperature.

The limit of the fast neutron dose level for the graphite reflectors is assumed to be around 3.0×10^{22} n/cm^2 (E> 0.1 MeV) [26], equivalent to 1.7×10^{22} n/cm^2 EDN. The fast neutron flux (E> 0.1 MeV) in the reflector of the DB HTR-PM is shown in Figure 36. The fast flux peak (4.5×10^{13} cm^{-2}s^{-1}) in the side reflector is comparable to that of UO$_2$ fueled HTR designs, such as the PBMR-400. In this latter annular core design the inner reflector is planned to be replaced after 18 years of operation, which is equivalent to a dose level of 2.6×10^{22} n/cm^2 for the region of the peak. Figure 36 shows that only a small part of the reflector in the DB HTR-PM will attain these high dose levels. Only 25% of the reflector will attain a dose level above 5.0×10^{21} EDN during the lifetime of the reactor (60 years). Therefore Cases 8 and 9 of Table 7 can be seen as very conservative cases.

The time point at which the maximum fuel temperature is reached, is significantly delayed with increasing reflector dose. The heat transferred to the RHRS is reduced, because the conductivity of the reflector is lower for the high dose levels. The reduced heat transfer is also reflected in lower CB and RPV temperatures. Therefore, it takes longer before the amount of decay heat generated is lower than the amount of heat removed from the reactor. This leads to a longer time that the core is heated up. For Cases 7-9 in Table 7, the maximum peak fuel temperature has not been reached within the 100 hour-time domain of the calculation.

Table 7. Impact of the fast neutron dose level on core parameters for a DLOFC transient.

Case	Case description	$T_{peak,max}$	$t_{peak,max}$	$T_{ave.,max}$	$T_{CB,max}$	$T_{RPV,max}$
1	Reference case.	1639°C	27.5 h	889°C	422°C	337°C
2	Temperature dependent Zehner-Schlünder.	1585°C	26.5 h	885°C	422°C	337°C
3	Same as Case 2, but DB decay heat curve.	1677°C	70.5 h	946°C	449°C	356°C
4	Same as Case 3, but dose level of *pebbles* is 1.0×10^{21} EDN.	1712°C	66.5 h	968°C	450°C	357°C
5	Same as Case 3, but dose level of *pebbles* is 2.0×10^{21} EDN.	1718°C	66.5 h	973°C	450°C	358°C
6	Same as Case 3, but dose level of *pebbles* is 2.5×10^{21} EDN.	1719°C	66.5 h	974°C	450°C	358°C
7	Same as Case 6, but dose level of *reflector* is 5.0×10^{21} EDN.	1877°C	100 h	1143°C	444°C	353°C
8	Same as Case 6, but dose level of *reflector* is 15.0×10^{21} EDN.	1931°C	100 h	1185°C	435°C	347°C
9	Same as Case 6, but dose level of *reflector* is 30.0×10^{21} EDN.	1948°C	100 h	1200°C	433°C	344°C
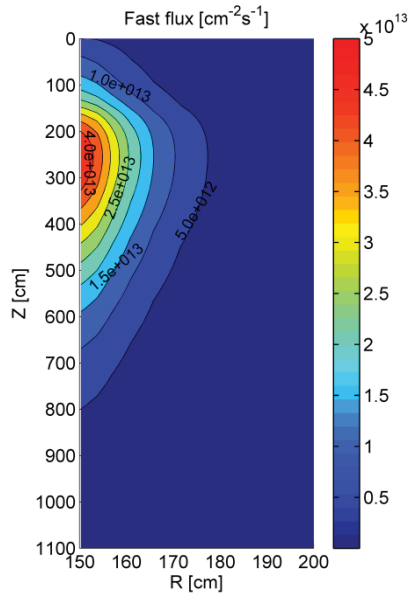
Figure 36. The fast neutron flux profile in the side reflector of the DB HTR-PM.

3.4.6   Impact of a Reduction in Reactor Power on the Core Temperatures

The reactor power of the DB HTR-PM has been varied in the DLOFC transient calculations to investigate the effect on the core temperatures. A fast neutron dose level of 2.5×10^{21} n/cm^2 EDN and 5.0×10^{22} n/cm^2 EDN for the pebbles and side reflector are assumed, respectively (Case 7 of Table 7). The decay heat curve for DB fuel was adopted. The helium mass flow has been kept constant for all cases.

Error! Not a valid bookmark self-reference. shows that the core peak and average temperature are approximately linearly dependent of the reactor power. The peak temperature can be reduced to 1600°C, which is the generally accepted fuel temperature limit, when the reactor power is reduced to 192 MW. Since the mass flow is kept constant in this study, this reduction in reactor power would also result in a reduction of the helium outlet temperature to 634°C. This outlet temperature could be increased in turn to 750°C by reducing the mass flow without significantly increasing the maximum temperatures during the DLOFC transient.

Table 8. Impact of reactor power reduction on the core temperatures during a DLOFC transient.

Case	$P_{reactor}$	$T_{peak,max}$	$t_{peak,max}$	$T_{ave.,max}$	$T_{CB,max}$	$T_{RPV,max}$
1	250.0 MW$_{th}$	1877°C	100 h	1143°C	444°C	353°C
2	237.5 MW$_{th}$	1816°C	100 h	1105°C	435°C	346°C
3	225.0 MW$_{th}$	1756°C	99.5 h	1067°C	426°C	340°C
4	212.5 MW$_{th}$	1697°C	95.5 h	1030°C	417°C	332°C
5	200.0 MW$_{th}$	1638°C	82.5 h	993°C	406°C	324°C
6	187.5 MW$_{th}$	1581°C	79.5 h	956°C	396°C	316°C

3.4.7   Conclusion on the DB HTR-PM Transient Analysis

The following conclusions can be made:

- The decay heat power of DB fuel is higher than that of UO_2 for the time domain t > 5 hours. As a result the maximum core peak and average temperatures during a DLOFC transient in the DB HTR-PM are higher (92°C and 61°C, respectively). Also, the time point of these maximum temperatures is delayed by 44 hours.

- The maximum temperatures during a DLOFC are sensitive to both the neutron dose level of the pebbles and the side reflector. For a best estimate value of the dose levels the maximum core peak temperature increases with an additional 200°C to 1877°C. It is noted here that this increase is also to be expected for the standard HTR-PM with UO_2 fuel and was not taken into account in Zhang et al.'s article [23].

- The high temperatures during the DLOFC in the DB core can be reduced to 1607°C by reducing the reactor power from 250 MW to 192 MW, while retaining a helium outlet temperature of 750°C. A more attractive way to reduce the maximum temperature might be achieved by increasing the number of pebble recirculation passes.

4.   FUEL PERFORMANCE ANALYSIS OF THE DEEP-BURN PEBBLE-BED REACTOR

4.1   Investigation of the Impact of CO Production and Oxygen Getter on the Particle Performance

In the FY 2009 fuel performance analysis, it was found that the production of CO in the DB coated particles can be detrimental to their integrity. However, in these analyses conservative values for the oxygen release per fission were used. Recent publication of thermo-chemical calculations [27] for the oxygen per fission released in Pu-fuel has been used in the current analyses. Results of the pressure in the coated particle fuel from CO production [27] are shown in Figure 37.
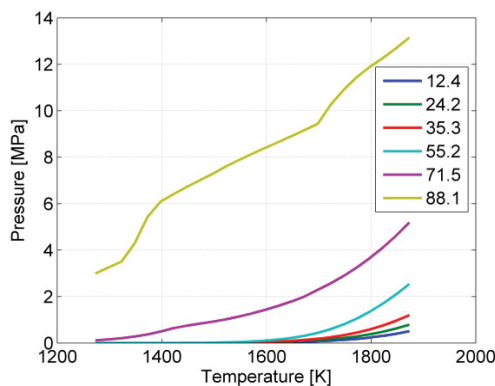
Figure 37. Pressure build-up in the buffer layer of a DB-coated fuel particle according to Besmann's article [27] as a function of the temperature (K) and burnup (% FIMA).

Very High Temperature Reactor (VHTR) Deep Burn Core and Fuel Analysis
Complete Design Selection for the Pebble Bed Reactor
9/21/2010

44

The data presented in Figure 37 is used to construct a table for the oxygen atoms per fission released as CO for implementation in the PASTA-coated particle stress analysis code. The following assumptions were made:

$$O/_f = \frac{n_{CO}}{n_{Pu+MA,0} \cdot FIMA} \tag{21}$$

with,

$$n_{CO} = \frac{pV_{buf}}{RT} \tag{22}$$

$$V_{buf} = \frac{4}{3}\pi\left(R_{buf}^3 - R_{ker\,n}^3\right)\left(1 - \frac{\rho_{buf}}{\rho_{graphite}}\right) \tag{23}$$

$$n_{Pu+MA,0} = \frac{\rho_{Pu+MA,0} \cdot V_{ker\,n}}{M_{Pu+MA,0}} \tag{24}$$

Table 9. Key characteristics of DB fuel assumed in the above equations.

R_{kern}	100 μm
R_{buf}	220 μm
ρ_{buf}	1.05 g/cm^3
$\rho_{graphite}$	1.8 g/cm^3
R	8.314 J/kg/K
$M_{Pu+MA,0}$	272 g/mol
$\rho_{Pu+MA,0}$	10.0 g/cm^3

Table 10. Oxygen atoms per fission released as CO in DB fuel as a function of the burnup and temperature.

T (K)/ FIMA (%)	12.4	24.2	35.3	55.2	71.5	88.1
1273	3.34E-06	2.68E-06	2.59E-06	2.39E-06	1.68E-03	3.51E-02
1298	5.90E-06	4.75E-06	4.62E-06	4.47E-06	2.21E-03	3.75E-02
1323	1.02E-05	8.22E-06	8.07E-06	8.16E-06	2.89E-03	3.96E-02
1348	1.72E-05	1.39E-05	1.38E-05	1.45E-05	3.82E-03	4.75E-02
1373	2.84E-05	2.30E-05	2.30E-05	2.52E-05	5.01E-03	5.92E-02
1398	4.60E-05	3.74E-05	3.77E-05	4.29E-05	6.50E-03	6.51E-02
1423	7.33E-05	5.97E-05	6.05E-05	7.13E-05	8.33E-03	6.74E-02
1448	1.15E-04	9.36E-05	9.55E-05	1.17E-04	9.49E-03	6.93E-02
1473	1.76E-04	1.45E-04	1.48E-04	1.88E-04	1.04E-02	7.11E-02
1498	2.67E-04	2.20E-04	2.27E-04	2.96E-04	1.13E-02	7.27E-02
1523	3.99E-04	3.29E-04	3.42E-04	4.59E-04	1.24E-02	7.46E-02
1548	5.88E-04	4.85E-04	5.07E-04	6.99E-04	1.36E-02	7.60E-02
1573	8.54E-04	7.05E-04	7.42E-04	1.05E-03	1.50E-02	7.74E-02
1598	1.22E-03	1.01E-03	1.07E-03	1.54E-03	1.65E-02	7.86E-02
1623	1.73E-03	1.43E-03	1.52E-03	2.24E-03	1.82E-02	7.96E-02
1648	2.42E-03	2.00E-03	2.13E-03	3.20E-03	2.00E-02	8.07E-02
1673	3.34E-03	2.77E-03	2.95E-03	4.49E-03	2.21E-02	8.18E-02
1698	4.55E-03	3.77E-03	4.03E-03	6.17E-03	2.48E-02	8.30E-02
1723	6.13E-03	5.07E-03	5.43E-03	8.32E-03	2.75E-02	8.90E-02
1748	8.16E-03	6.73E-03	7.22E-03	1.10E-02	3.05E-02	9.32E-02
1773	1.07E-02	8.84E-03	9.46E-03	1.42E-02	3.38E-02	9.65E-02
1798	1.40E-02	1.14E-02	1.22E-02	1.80E-02	3.75E-02	9.88E-02
1823	1.80E-02	1.46E-02	1.55E-02	2.23E-02	4.16E-02	1.01E-01
1848	2.28E-02	1.84E-02	1.94E-02	2.71E-02	4.61E-02	1.03E-01
1873	2.86E-02	2.29E-02	2.38E-02	3.23E-02	5.10E-02	1.05E-01

It is noted that the numbers in Table 10 are significantly lower than the experimental *O/f* results reported in Horsley et al.'s article [28]. However, the latter reference deals with a different initial oxygen stoichiometry (UO_2 instead of $PuO_{1.7}$), which might account for the difference.

The sensitivity of the stresses in the coatings to the approximation for CO modeling has been investigated. The following four different assumptions for CO production have been considered:

1. An empirical relation for the production of free oxygen per fission that is widely used for UO_2 fuel [29].

2. A conservative fixed value of 0.4 for the number of free oxygen atoms per fission.

3. The data presented in Table 10 based on thermo-chemical calculations for Pu-fuel [27].

4. A zero production of CO, which would be equivalent to a particle in which all free oxygen is gettered.

The effect of the above stated modeling assumptions on the SiC stress history is shown in Figure 38. The data of Table 10 predicts a minimal contribution of CO to the internal pressure of the coated particle with a negligible impact on the SiC stress. This shows that using the correlation from Proksch et al. [29] or a value of Ox/f= 0.4 is conservative. It is noted that data from Table 10 gives significant contribution of CO to the pressure for higher burnup values or higher temperatures. The latter could be experienced during transients.
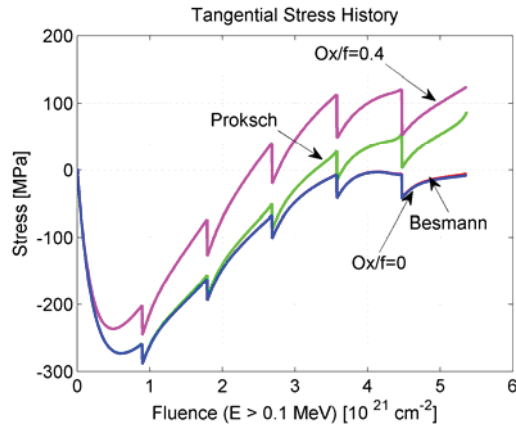
Figure 38. Impact of the CO modeling assumption on the SiC tangential stress history. The result for the stress obtained with the data of Table 10 [27] is denoted with Besmann and the result obtained with the data from Proksch et al.'s article [29] with Proksch.

4.2   Investigation of the Impact of the Variation in the Pebble Location and in the Thicknesses of the Particle Coatings on the Performance

The PASTA code has been further improved to allow for the evaluation of coating stresses during slow transients such as an LOFC incident in the Deep Burn Pebble Bed core. Furthermore, the code is now capable of treating the statistical variation in the coating thicknesses and calculating the coating stress as a function of the pebble position in the core.

The following sections show the stress affects of the radial core position and the variation in the size of the coatings, as well as the influence of the free oxygen per fission. In Section 4.3 the performance during the LOFC transient conditions is presented. Section 4.3 concludes on the overall performance of the two types of fuel investigated for the different cases.

4.2.1   SiC Coating Stress as a Function of the Pebble Location

A fuel performance analysis is performed that takes into account the fuel temperature variation in the radial direction of the core. Figure 39 shows 2-D core distribution maps of the maximum SiC stress in the particles. The results show that the pebbles near the radial edges of the pebble bed, which have high temperatures, contain particles that have a significant higher SiC stress as compared to the average particle.
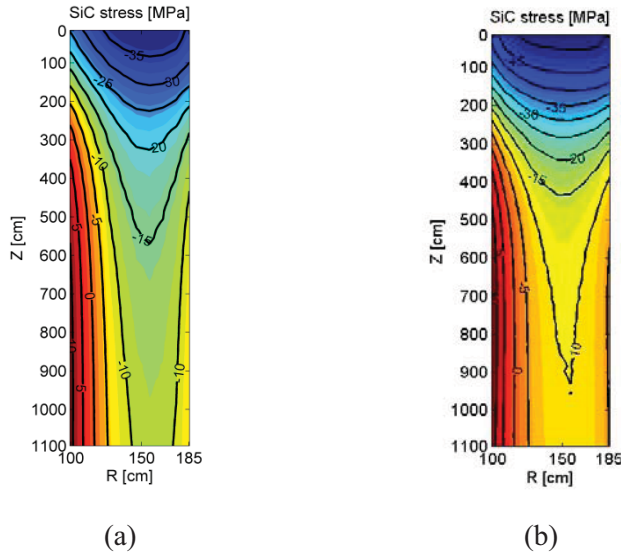
Figure 39. SiC coating stress, for a pebble that has been (re)introduced in the core 6 times, as function of the position the DB core at nominal conditions for the Pu-only (a) and the Pu+MA (b) fueled designs.

4.2.2   Effect of Variation of the SiC and Carbon Buffer Layer Thickness

The coatings and kernel of TRISO-coated fuel particles vary slightly in size (thickness) depending of the fabrication process and quality control procedure of the process. A variation in the coating dimensions from the reference values has an effect on the particle performance. For example, a reduction of the buffer layer results in less room to accommodate the gaseous fission products and therefore an increase in the buffer pressure. This leads to higher stresses in the other coating layers with a higher failure probability as a result.

As a result of the non-linear behavior of the mechanical stresses during irradiation, the stress state and failure probability of the average coated particle, that has the exact dimensions of the design specifications, is not necessarily equal to the average stress state of all the various particles, which show small deviations from exact specifications.

If the distributions $f(x_1),\ldots,f(x_n)$ of (the variation of) the coating thicknesses $x_1,\ldots,x_n$ are known, the consequent expected stress state E can be calculated from the distribution functions and a stress function $\sigma(x_1,\ldots,x_n)$:

$$E[\sigma(x_1,\ldots,x_n)] = \int_{a_n}^{b_n}\ldots\int_{a_1}^{b_1}\sigma(x_1,\ldots,x_n)f(x_1)\ldots f(x_n)dx_1\ldots dx_n \tag{25}$$

Note that it is assumed that the probability density functions are independent. Similarly, the expected failure probability of all the various particles can be calculated replacing the stress function $\sigma(x_1,\ldots,x_n)$ by the failure probability function $\psi(\sigma(x_1,\ldots,x_n))$, which predicts the failure probability as a function of a given stress state. Using this function and rewriting Equation (1) as a function of discrete points results in:

$$E[\psi(\sigma(x_1,\ldots,x_n))] = \sum_{x_n}\ldots\sum_{x_1}\psi(\sigma(x_1,\ldots,x_n))p(x_1)\ldots p(x_n) \tag{26}$$

The above integral is calculated in the PASTA code. The failure probability ($\psi(\sigma(x_1,\ldots,x_n))$) for given particle dimensions is calculated from the coating stresses. This probability is weighted with the probability of the particle having these dimensions ($p(x_1)\ldots p(x_n)$). By dividing the domains of the coating thicknesses in discrete parts, evaluation and summation of the probabilities, the expected failure fraction of all the particles combined ($E[\psi(\sigma(x_1,\ldots,x_n))]$) is obtained.

A PASTA calculation has been performed assuming Weibull distributions for the SiC and carbon buffer layer thickness (μ_{SiC}=45 μm, σ_{SiC}= 5 μm and $\mu_{C_{buf}}$=90 μm, $\sigma_{C_{buf}}$ = 5 μm). The failure probability of the SiC layer as a function of the SiC and carbon buffer thickness has been calculated assuming either a time and temperature dependent function or a more conservative value of O/f = 0.4 for the free oxygen production.

(a)[O/f (t,T)]   (b)[O/f : 0.4]
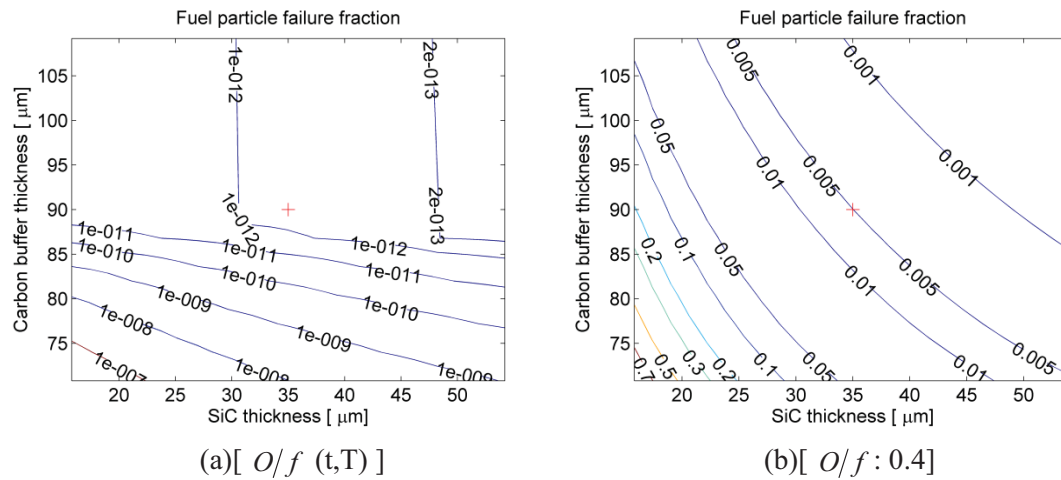
Figure 40. SiC failure probability for the Pu-fueled DB core as a function of the buffer and SiC coating thickness assuming (a) O/f as a function of the irradiation time and temperature; and (b) for a fixed value of O/f =0.4 (b).

It can be seen that for O/f (t,T) the particle failure probability remains low for all coating dimensions with an overall failure probability of $3.8\cdot 10^{-11}$. However, if a more conservative value of O/f = 0.4 is assumed high failure probabilities can be expected with an overall value of $8.0\cdot 10^{-3}$.

4.3   Transient Analysis of the Fuel Performance during a Loss Of Forced Cooling Incident

During an LOFC incident, the center part of the core can be expected to reach considerably higher temperatures as compared to the nominal values. The pressure in the buffer layer is directly dependent on the temperature, but also indirectly through the diffusion of fission products and CO production. Furthermore, the stress in the SiC layer is a function of the thermal expansion of the SiC layer itself and the PyC layers.

An LOFC transient calculation has been performed using a standalone thermal-hydraulics calculation in PEBBED. Figure 41 shows the core maximum fuel temperature history of an LOFC transient and core temperature profile at the time point of the maximum temperature (t = 47 h).

The stress calculation procedure for the transient is as follows:

1. For each point in the lifetime (irradiation dose and time) of the coated particle fuel, the stresses in the coatings are calculated assuming normal operation of the reactor. The histories of the fuel temperature, fission product build-up, irradiation time, and fast fluence (E > 0.1 MeV) during the lifetime of a pebble are generated with PEBBED by calculating the equilibrium core.

2. The fuel temperature history for each position in the core is generated by a DLOFC transient calculation in THERMIX. In this transient, the temperature difference between pebble surface and pebble center is small as compared to normal reactor operation, since the heat production is determined by the decay heat only. Therefore, it is assumed that for a given location in the core pebbles with a different burnup class (i.e., representing different points in the lifetime of the pebble) experience the same temperature history during the transient.

3. The temperature history of a pebble now consists of two parts. The first part represents normal reactor operation, in which the pebble reaches a given point in life at which the transient occurs. At this point the pebble has passed several times through the core and has reached a certain core position. The second part of the pebble temperature history is determined by the temperature that this core location has during the transient (Figure 42).

4. For each position in the core the six possible temperature histories are used to calculate the corresponding histories for the pressure build-up in the buffer layer.

5. The stress state of the coatings is calculated during the entire lifetime (normal operation plus the transient part) of the pebbles (Figure 42).
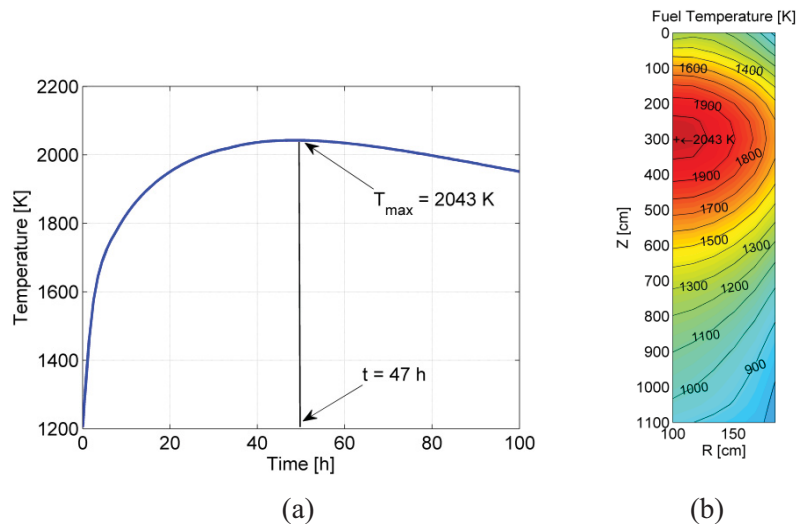
Figure 41. (a) Core maximum fuel temperature history; and (b) the fuel temperature profile at the time of the maximum temperature.

(a)   (b)
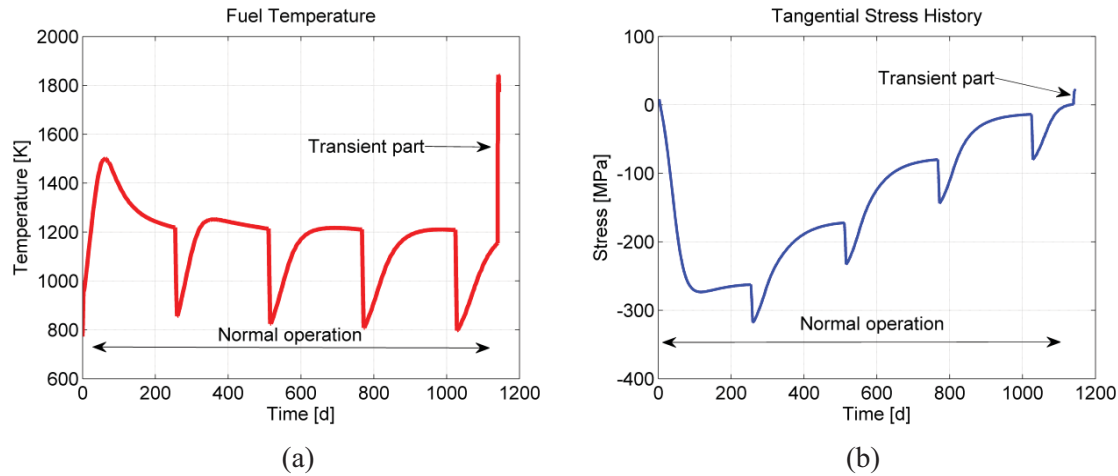
Figure 42. Temperature and stress history for a pebble that has been (re)loaded in the core 5 times and is location in the top region of the core. The increase in temperature during the 100-hour-long LOFC transient results in an increase of the SiC stress.

The behavior of the buffer pressure and the resulting SiC during the transient for several axial core positions is shown in Figure 43. It can be seen that for some positions the buffer pressure and SiC significantly increase during the transient, which increase the failure probabilities of the particles in the respective core regions.

(a)   (b)
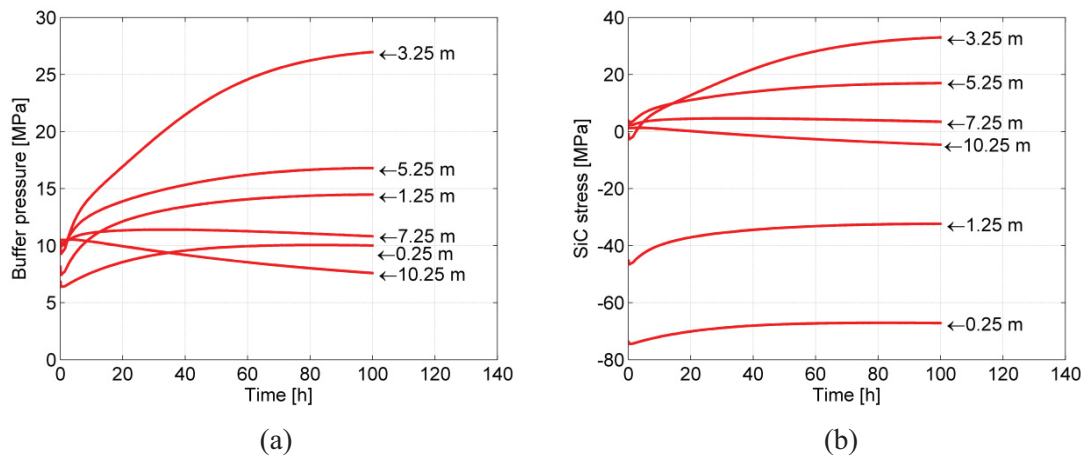
Figure 43. (a) Pressure and (b) SiC stress history for several axial core positions during a DLOFC transient.

4.3.1   DB Pebble Bed Fuel Performance Conclusions

The fuel performance of DB fuel has been investigated using the improved PASTA-PEBBED code system for coated particle stress analysis. The predicted failure fractions for the different cases are presented in Table 11.

Table 11. Fuel failure probabilities.

Fuel type	Nominal conditions		LOFC transient
	O/f : (t,T)	$O/f = 0.4$	O/f : (t,T)
Pu	3.8×10^{-11}	8.0×10^{-3}	2.6×10^{-4}
Pu + MA	5.7×10^{-16}	1.9×10^{-3}	9.4×10^{-7}

It was found that the average (reference dimensions and average core radial temperature) fuel particle performs well. However, if a more conservative value for O/f is assumed significant fuel failure can be expected, especially for LOFC conditions. To reduce failure probability, an improved fuel or core design is desirable for the DB pebble bed reactor.

4.4 Inter-comparison of Fuel Performance Codes Fuel Coated Particle Stress Analysis

In the framework of the DB project, several codes (PASTA, COPA, and PISA) have been used to analyze the durability of the coated particle fuel for different cases.

The PASTA [8], COPA [30], and PISA [31,32] codes have been used in a fuel performance comparison through collaboration between INL, General Atomics, and the Korea Atomic Energy Institute [33]. The comparison is presented in the following sections.

The codes employ different models and assumptions for the analysis of the coated particle performance. These differences can be found in the models for stress analysis on the various layers of the TRISO particle, models for fission products release, migration and accumulation within the TRISO particle, models for free oxygen and CO formation and migration, models for temperature field within the various layers of the TRISO particle, and models for the prediction of failure rates. Moreover, the possibility of different constitutive data for mechanical and thermal properties make it highly unlikely that the three codes would give identical results in the modeling of identical situations.

An inter-comparison has been carried out by the cooperating institutions within the workscope of the Department of Energy (DOE) Deep-Burn Project, using a common set of predefined TRISO conditions (burn-up levels, temperature or power levels, etc.). The coated particle under investigation is a design that is currently considered within the Deep-Burn Project to be fabricated within the near future. Besides the inter-comparison of the results for the performance of this fuel design additional investigations are performed to quantify the sensitivity of the input parameters. Finally, conclusions are drawn regarding both the performance analysis methods and the performance of the envisioned DB particle design.

4.4.1 Description of the DB Coated Particle Design used for Code-to-code Comparison

The coated particle design specifications used for the inter-comparison are derived from the particle design that is considered to be fabricated in the near future within the Deep-Burn Project. The fuel kernel consists of TRUs and a SiC getter that reduces the CO production in the particle. The mole ratio of TRU:SiC in the kernel is 1:0.6, having an average density of 7.6 g/cm^3. The MA oxide (MAO2−x) fuel is sub-stoichiometric having 1.8 oxygen atoms per MA atom on average. The isotopic compositions of the TRUs are shown in Table 12. Table 13 shows the dimensions of the kernel and coating layers and their statistical variation in size.

Table 12. Isotopic composition of Deep-Burn fuel.

Isotope	Fraction (wt%)
Np-237	6.8
Pu-238	2.9
Pu-239	49.38
Pu-240	23
Pu-241	8.8
Pu-242	4.9
Am-241	2.8
Am-242m	0.02
Am-243	1.4

Table 13. Dimensions of the coating layers and its statistical variation for the DB coated particle design.

Layer	Thickness (µm)	Density (g/cm3)
Kernel $(MAO_{1.8}(SiC)_{0.6})$	350*±10	7.6
Buffer	100±5	1.0
IPyC	35±5	1.9
SiC	45±5	3.2
OPyC	35±5	1.9

*Kernel diameter.

To compare the fuel performance codes predefined boundary conditions (Table 14) are adopted instead of using core analysis tools. It is assumed that the fuel particle has a fixed (outer surface) temperature of 1200 K at a power level of 2.0×10^{-2} W for 1120 days of irradiation in the core. The temperature within the kernel and in the coating layers is calculated by the fuel performance codes from the particle surface temperature and kernel power. At the end of the irradiation the particle reaches a burn-up level of 560 MWd per kilogram of initial heavy metal (IHM) loading. The adopted parameters are taken from a PEBBED analysis of a Pebble Bed Modular Reactor design (400 MWth) loaded with DB fuel (Table 12) [34]. In the inter-comparison case, the fuel burn-up and the fast neutron fluence level attained, are linear functions of the irradiation time, since the kernel power level is assumed to be constant. It is noted that the boundary conditions presented above are intended to represent the typical environment of a DB reactor core without making any specific assumptions about the type of reactor (pebble bed or prismatic).

Table 14. Assumptions and boundary conditions adopted in the fuel performance analysis.

Final burn-up level	560 MWd/kg IHM
Final fast fluence (E > 0.1 MeV)	5.0×10^{21} cm^{-2}
Particle surface temperature	1200 K
Kernel power	2.0×10^{-2} W
Irradiation time	1120 days

In the following section (Section 4.4.2), the results of the fuel performance analysis of the three codes are compared and analyzed. In Section 4.4.3 the sensitivity of several input parameters on the results is investigated.

4.4.2   Analysis of the Reference Coated Particle

During the irradiation of the coated particle fuel gaseous fission products that are formed in the kernel diffuse to the porous carbon buffer layer. Figure 44 shows the amount of fission products released from the kernel to the buffer layer as a function of the fast neutron fluence attained. The PASTA and COPA codes assume the release according to the Kidson and Booth models [12], in which the diffusion of the fission products is a function of the time and the temperature, PISA assumes a fixed value of 60% release fraction. As a result, the PISA code gives a linear build-up of the fission products in the buffer layer, while in the PASTA and COPA codes the release is somewhat delayed (Figure 45). It is noted that no formation of CO by free oxygen is expected, since the kernel contains a SiC getter. Furthermore, the contribution of He is assumed to be negligible.

The calculation results for the available (void) volume for the gaseous fission products is shown in Figure 46. In the PASTA and PISA codes the initial void volume in the buffer is calculated according to:

$$V_{void} = 1 - \frac{\rho_{buf}}{\rho_{graphite}}$$ (27)

in which, ρ_{buf} is the buffer density and $\rho_{graphite}$ is the theoretical maximum value of the density of graphite. The COPA code assumes that the kernel volume also has some void space (0.5% of the kernel pore volume). Furthermore, the PISA and COPA codes assume that the void space in the buffer reduces with increasing radiation due to kernel swelling, which is caused by build-up of solid and gaseous fission products.

The build-up of gaseous fission products in the buffer results in a pressure (Figure 47) on the IPyC layer, which is calculated by all three codes by the Redlich-Kwong equation of state. The pressure is directly dependent on the buffer void volume. Therefore the PISA code calculates the highest pressure and the PASTA code the lowest, resulting from the low and high values for the void volume, respectively.

In principle, the buffer pressure results in a tangential tensile stress on the SiC layer, which is the main load-bearer of the particle. However, the PyC layers shrink (Figure 48) and thereby put the SiC under compression. The following references and assumptions were used by the codes to determine the PyC dimensional change as a function of the fast fluence level:

- COPA: Reference [15], with $\rho_{PyC} = 1.9$ g/cm^3, T = 1200 K, BAF$_0$=1.0
- PASTA: Reference [15], with $\rho_{PyC} = 1.9$ g/cm^3, T = 1200 K, BAF$_0$=1.036
- PISA: Reference [35] page 30, with T = 1473 K, BAF$_0$=1.036.

The shrinkage and swelling behavior of the PyC layers is a function of the BAF, which is determined by the fabrication process of the layers. For a PyC layer that is isotropic (BAF = 1), the dimensional change in the radial and tangential dimensions are equal, which is assumed in the COPA code. The PASTA and PISA codes assumed that the PyC is slightly anisotropic (BAF = 1.036), which results in less shrinkage of the PyC in the radial direction in the beginning of the irradiation. Furthermore, there exists a turnaround point where the shrinkage in the radial direction turns into swelling. It is noted that the effective length of the PyC layers in the tangential direction is significantly larger than the radial one, which makes the dimensional change behavior of the first, the more important.

In the beginning of the irradiation of the particle, the dimensional change of the PyC determines the stress state of all three layers (IPyC, SiC, and OPyC) entirely (Figure 49–Figure 51). Since the three codes use

Very High Temperature Reactor (VHTR) Deep Burn Core and Fuel Analysis
Complete Design Selection for the Pebble Bed Reactor
9/21/2010

54

similar dimensional change rates of the PyC in the tangential direction there is good agreement between the codes for the calculated stresses for low fluence levels. With increasing fluence level some differences can be identified, which can be explained as follows. The PASTA code has a lower buffer pressure than the COPA code, resulting in a lower stress on the SiC layer at the end of the irradiation. The PISA code has a higher buffer pressure than PASTA, but this seems to be compensated by the higher shrinkage (tangential) rate of the PyC. Therefore the PASTA and PISA codes show a similar result for the final SiC stress at the end of the irradiation.

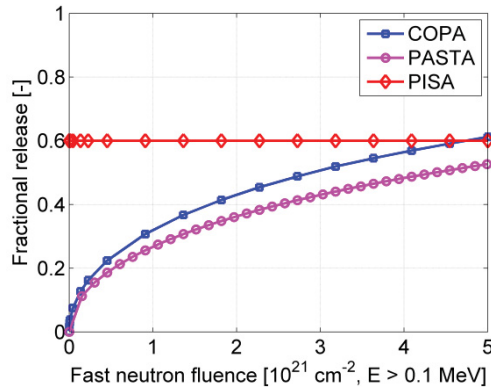Figure 44. Fractional release of gaseous fission products from the fuel kernel to the buffer layer, calculated by the COPA, PASTA, and PISA codes.
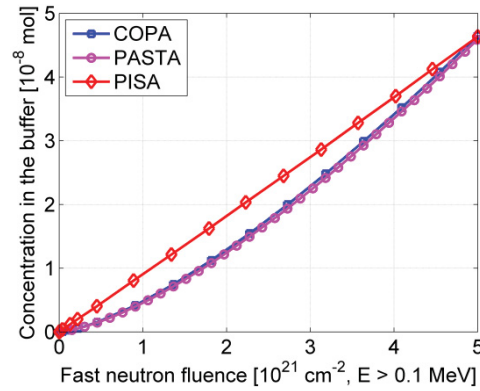
Figure 45. Concentration of Xe and Kr in the buffer layer calculated by the COPA, PASTA, and PISA codes.

Figure 46. Void volume in the buffer layer calculated by the COPA, PASTA, and PISA codes.

Figure 47. Buffer pressure calculated by the COPA, PASTA, and PISA codes.
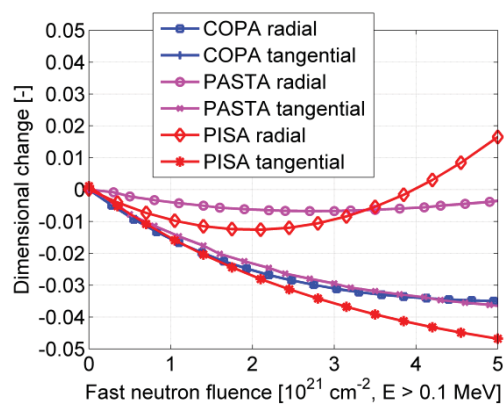
Figure 48. Correlations for the PyC dimensional change

Figure 49. Tangential stress in the IPyC layer calculated by the COPA, PASTA, and PISA codes.

Figure 50. Tangential stress in the SiC layer calculated by the COPA, PASTA, and PISA codes.

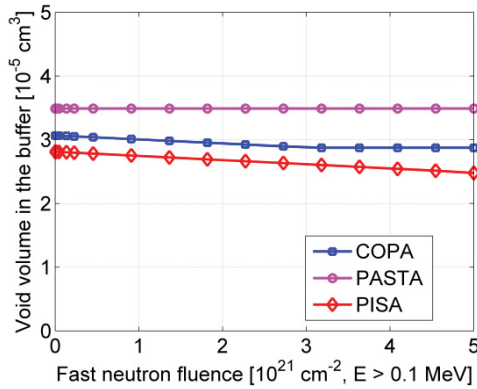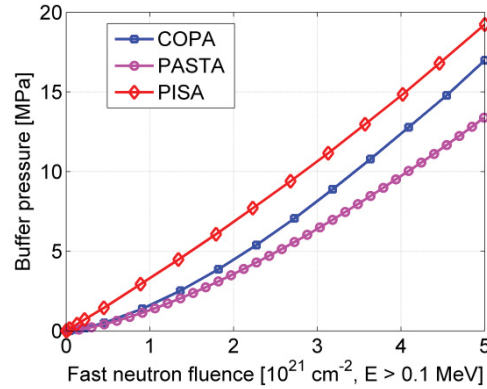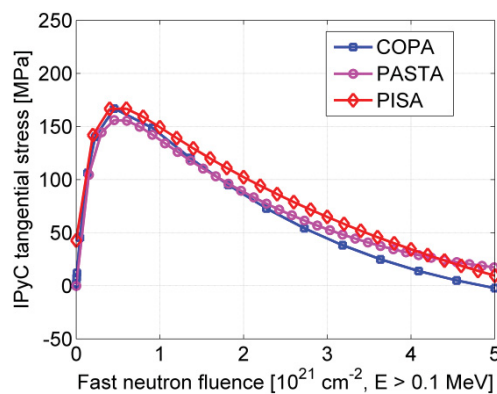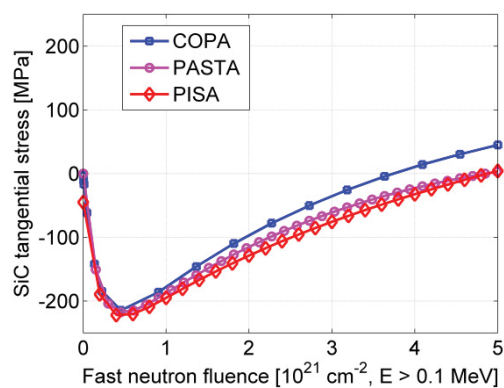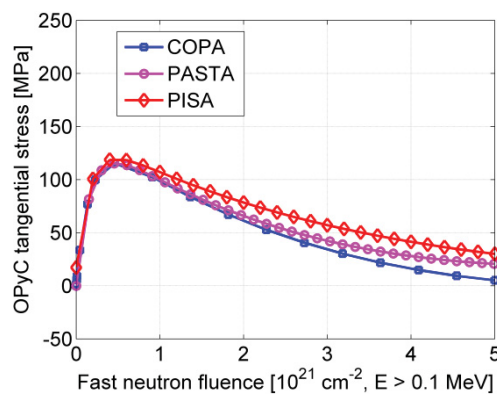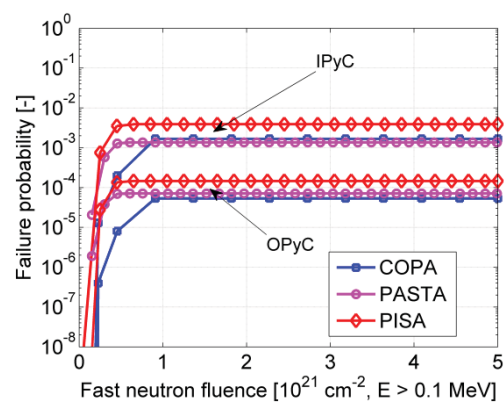Figure 51. Tangential stress in the SiC layer calculated by the COPA, PASTA, and PISA codes.

Figure 52. Cumulative failure probability of the IPyC and OPyC coating layers as a function of the fast fluence calculated by the COPA, PASTA, and PISA codes.

There is a relatively good agreement between the failure probabilities of the three codes (Figure 52), because the maximum IPyC and OPyC stresses are similar. Although the failure probability of the IPyC layer is relatively high, no significant failure probability was found for the SiC layer. While the PASTA and PISA codes calculated the failure probabilities directly from the stress levels, the COPA code performed a Monte-Carlo calculation to determine the failure probability.

4.4.3   Sensitivity of Input Parameters on Fuel Performance

In the previous section some differences in the findings were found resulting from the various assumptions made in the codes. Especially, the buffer void volume and the dimensional change of the PyC layers were modeled differently, which led to a small spread in the results of the coating stresses and the failure probability. To quantify the sensitivity of several input parameters on the coating stress and failure probability of the layers additional studies have been performed. The following parameters have been investigated:

- The available volume (void) for the fission products in the buffer and kernel

- The particle coating dimensions

- The dimensional change of the PyC layers

- The creep coefficient of the PyC layers.

The effect of the variation in the thickness of the SiC and buffer layer has been investigated with the PASTA code. The two layers were allowed to vary around their average value, assuming a normal distribution with a standard deviation of 5 μm, according to Table 13. The failure probability for a given set of coating dimensions was weighted with its probability of occurrence. It was found that the variation in coating size did not have a large impact on the average failure probability of the SiC layer.

The failure probability of this batch of particles was found to be $<1\times 10^{-9}$.

An analysis was made with the PASTA code using three different BAF values, which correspond with three different PyC irradiation induced dimensional change rates for the radial and tangential direction (Figure 53). It can be seen from Figure 54 that especially the final stress level of the SiC layer is sensitive to the dimensional change of the PyC, while the maximum stress of the IPyC and OPyC is relatively insensitive. This conclusion appears to be at variance with observations during irradiations and to the importance usually assigned to the BAF_0 of pyrocarbon coatings.

From the analysis in the previous section it was found that the maximum stress in the PyC layers (170 MPa) is relatively close to its median strength (300 MPa). This is expected to be the result of a relatively low value of the creep coefficient for radiation induced creep. An additional case was investigated with the PISA code in which the creep coefficient was doubled. The results for the coating stresses are shown in Figure 55. It can be seen that the increased creep coefficient reduces the effect of the dimensional change of the PyC layers. The tangential stresses are lower in all three layers for the increased creep coefficient case, while the SiC stress at the end of the irradiation is higher.

The PASTA code has been used to investigate the sensitivity of the void volume in the buffer on the SiC stress. Results are shown in Figure 56. It can be seen that a reduction of the void volume significantly increases the SiC, while an increase of the void volume only results in a moderate reduction of the stress.
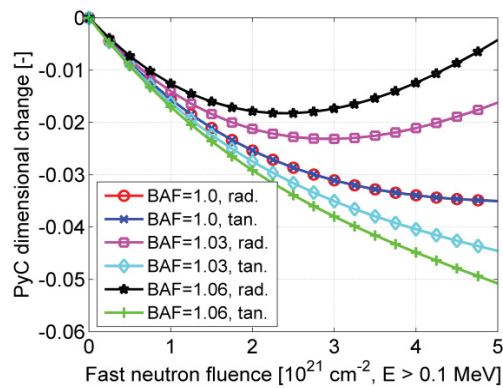
Figure 53. Irradiation induced dimensional change as a function of the fast fluence level (E > 0.1 MeV) for three BAF values (1.00, 1.03, 1.06).
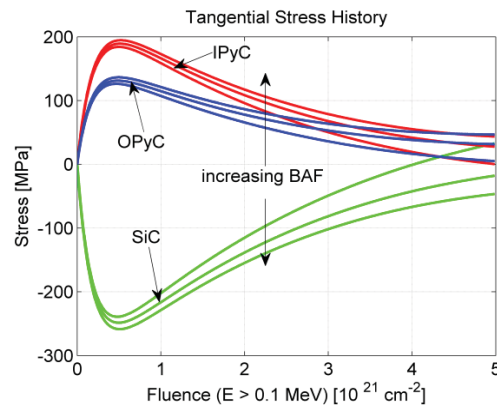
Figure 54. Effect of the BAF value (1.00, 1.03, 1.06) on the stresses in the coating layers (IPyC, SiC, OPyC) during irradiation.
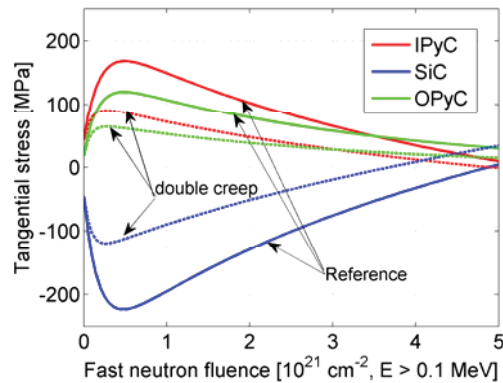
Figure 55. Tangential stress as a function of the fast fluence calculated by the PISA code, assuming either the reference value for the creep coefficient $(2.0 \times 10^{-29}(\text{MPa.m}^{-2})^{-1})$ or double this value.
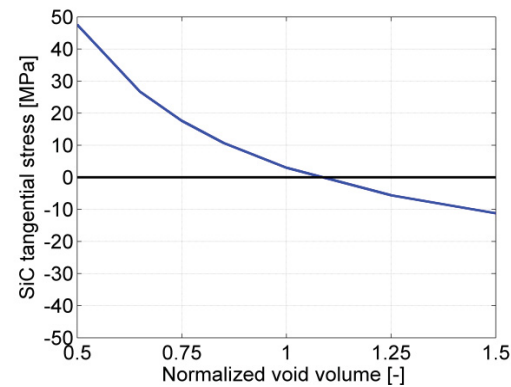
Figure 56. The maximum stress in the SiC layer during the irradiation as a function of the void volume in the buffer calculated with the PASTA code (reference volume = $3.5 \times 10{-}6$ cm^3).

4.4.4 Conclusions Regarding Fuel Performance Modeling of Deep-Burn Coated Particles

An inter-comparison of the fuel performance modeling of DB-coated particle fuel has been performed. It was found that there are several differences in the modeling approach between the COPA, PASTA, and PISA codes.

- The models for the void volume in the kernel and buffer layer to which the fission products diffuse differ slightly between the codes. In the PISA and COPA models, the kernel is assumed to expand as a function of the irradiation level, thereby reducing the buffer void volume. Therefore, the buffer pressure in these models is higher, which results in a higher SiC stress.

- The dimensional change of the PyC layers has a large impact on the stress state of the coating layers. For a coated particle design that has a sufficient buffer volume to accommodate the fission products, the dimensional change determines the stress state of the coatings almost entirely.

- The effect of the dimensional change of the PyC layer is reduced in case the layers exhibit significant radiation induced creep. Proper experimental data on PyC radiation induced strain creep is key to accurate prediction of coated particle performance.

5.   CONCLUSIONS

Conclusions Regarding the Analysis and Design of the Deep-Burn Pebble-bed Core

Subtask 1.1: Improvement of the temperature reactivity coefficient

To improve the moderator temperature coefficient both the addition of Er-167 to the pebble or fuel kernel as well as an increasing the fuel loading per pebble have been considered. It was found that the Uniform Temperature coefficient can be rendered negative for the entire core and for the entire temperature domain by the addition of Er-167 to the fuel kernel. The resulting penalty on the achievable discharge burnup is ~100 MWd/kg. This would result in an achievable discharge burnup of 600 MWd/kg for the Pu-only fuel.

Analysis in which the location of the Erbium within the pebble was varied, showed that the Erbium could be effectively (self-) shielded in the beginning of the irradiation. In doing so more Erbium would be available at high burnup, where it would be most effective in improving the temperature coefficient.

Alternatively to Erbium addition, the analysis shows that increasing the HM load from 2 to 3 g per pebble without burnable poison addition is the most attractive option with regard to the discharge burnup. It would keep the discharge burnup above 690 MWd/kg, while keeping the maximum UTC below -1 pcm/K.

Subtask 1.2: Reduction of the power and temperature peaking in the core

To avoid power peaking in the core both an annular core with a transparent inner reflector and a cylindrical core yield an improvement. However, the first alternative demands a low effect graphite density ($\rho < 0.2\rho_0$), which might be difficult to achieve in practice. The latter demands a reduction in the total reactor power, since cylindrical cores are less effective in heat removal during a Depressurized Loss Of Forced Cooling (LOFC) event.

It was found that an alternative Deep-Burn design based on the cylindrical HTR-PM (250 MWth) can achieve a higher discharge burnup of 560 MWd/kg (using a Pu and MA initial fuel loading). This design also exhibits lower temperature peaking (1190 K) during the first pebble pass. The maximum fuel temperature during a LOFC transient is with a best estimate value of 1734 K within generally accepted safety limits. It is noted that these temperature reductions are achieved at the expense of a lower helium outlet temperature (750°C), a lower reactor power (250 MW) and an increase of the number of pebble (re)circulation passes from 6 to 20.

Subtask 1.3: Analysis of the decay heat from Deep-Burn fuel

The decay heat curve of Deep-Burn fuel is similar to that of 'standard' UO_2 fuel in for low burnup levels.

At high burnup levels B > 600 MWd/kg it is significantly influenced by the contribution of the unstable minor actinides. These nuclides give a relatively large contribution for these burnup levels, especially after several hours of decay (t > 2 hours). The decay heat curves of the two Deep-Burn fuels considered are very similar. Because the Pu only fuel is able to attain a higher discharge burnup level the decay heat is also higher for this fuel type. From the transient analysis of a DB HTR-PM design it was found that adopting a typical DB decay heat curve instead of the standard curve for UO_2 fuel would increase the maximum fuel temperature by ~100 K. It is noted here that a fixed power profile was assumed for the decay heat during the transient. This is expected to be a conservative assumption, because the decay heat core power profile will be more flattened with increased cooling time.

Subtask 1.4: Analysis of the sensitivity of the fuel temperature on the fast neutron dose

The impact of the fluence level on the fuel temperature during normal and Loss Of Forced Cooling conditions has been determined. The maximum temperatures during a DLOFC are sensitive to both the neutron dose level of the pebbles and the side reflector. For a best estimate value of the dose levels the maximum core peak temperature increases with an additional 200°C to 1877°C. It is noted here that a similar increase is also to be expected for the 'standard' HTR-PM with UO_2 fuel.

Conclusions Regarding the Analysis and Design of the Deep-Burn Coated Particle Fuel

Subtask 2.1: Investigation of the impact of CO production and oxygen getter on the particle performance

Recently published data of CO production in Pu-fuel has been implemented in the PASTA stress analysis code. The data predicts a minimal contribution of CO to the internal pressure of the coated particle with a negligible impact on the SiC stress during normal operation. However, it is noted that for higher temperatures and burnup levels a significant contribution of CO to the pressure is to be expected. The latter could be experienced during transients. Therefore, the use of an oxygen getter is still recommended.

Subtask 2.2: Investigation of the impact of the variation in the thicknesses of the particle coatings and the pebble core location on the performance

The impact of the variation in coating thicknesses and the location of the pebble in the core on the fuel performance was investigated. A statistical analysis that takes into account the variation of the buffer layer and the SiC layer thickness was performed. It revealed that particles that have both a small buffer and a thin SiC layer have a high probability to fail. However, the probability of this combination is small and therefore does not contribute significantly to the average failure rate of a batch of particles.

The radial location of the pebble within the core showed small variations in the corresponding coating stress level. A maximum variation of $\Delta\sigma = 25$ MPa was observed. This does not lead to a significant increase in the particle failure fraction as compared to using the radial average pebble temperature, since the SiC layer remains under low tensile stress levels.

Subtask 2.3: Transient analysis of the fuel performance during a Loss of Forced Cooling incident

During a Loss Of Forced Cooling event in the reactor the fuel temperatures in some core regions are considerable higher than during normal operation. This results in an increase of the coating stresses and resulting particle failure. The failure fraction for Pu-only and Pu+MA fuels was 2.6×10^{-4} and 9.4×10^{-7}, respectively.

Subtask 2.4: Inter-comparison of fuel performance codes fuel coated particle stress analysis

The result of the COPA, PASTA and PISA codes were compared for the analysis of a DB coated particle design that includes an oxygen getter. All three codes predicted no significant through coating failure. The stress results were found to be sensitive to the dimensional change and creep of the PyC layers.

6. REFERENCES

[1] Versluis, R. M., F. Venneri, D. Petti, L. Snead, and D. McEachern, 2008, "Project Deep-Burn: Development of Transuranic fuel for High-Temperature Helium-Cooled Reactors," *Proc. of the 4th International Topical Meeting on High Temperature Reactor Technology (HTR2008), Washington DC, USA, 2008*.

[2] Reitsma, F., 2004, "The Pebble Bed Modular Reactor Layout and Neutronics Design of the Equilibrium Cycle," *In Proceedings of PHYSOR-2004, Chicago, USA, April 25-29, 2004*.

[3] Reitsma, F. et al., 2006, "The OECD/NEA/NSC PBMR Coupled Neutronics/Thermal Hydraulics Transient Benchmark: The PBMR-400 Core Design," *In Proceedings of PHYSOR-2006, September 2006, Vancouver, Canada.*

[4] Terry, W. K., H. D. Gougar, and A. M. Ougouag, 2002, "Direct Deterministic Method for Neutronics Analysis and Computation of Asymptotic Burnup Distribution in a Recirculating Pebble-Bed Reactor," *Annals of Nuclear Energy*, **29**, p. 1345–1364, 2002.

[5] ORNL, 2009, *SCALE-6: A Modular Code System for Performing Standardized Computer Analyses for Licensing Evaluations*, ORNL/TM2005/39, Version 6.0, Vols I-III, ORNL, 2009.

[6] Teuchert, E., et al, 1994, "V.S.O.P. – Computer Code System for Reactor Physics and Fuel Cycle Simulation," Forschungszentrum Jülich GmbH Jül-2897, 1994.

[7] Goluoglu, S., 2006, "Analysis of a Computational Benchmark for a High-Temperature Reactor Using SCALE," *Proceedings of PHYSOR 2006*, *Vancouver, BC, Canada, September 10–14, 2006*.

[8] Boer, B., A. M. Ougouag, J. L. Kloosterman, and G. K. Miller, 2008, "Stress analysis of coated particle fuel in graphite of High-Temperature Reactors," *Nuclear Technology*, **162**, p. 276–292, 2008.

[9] Jonnet, J., J. L. Kloosterman and B. Boer, 2008, "Development of a stress analysis code for TRISO particles in HTRs," *International Conference on the Physics of Reactors, Nuclear Power: A Sustainable Resource, Switzerland, 2008*.

[10] Snead, L. L., T. Nozawa, Y. Katoh, T-S. Byun, S. Kondo, and D. Petti., 2007, "Handbook of SiC properties for fuel performance modeling*,*" *Journal of Nuclear Materials*, **371**, p. 329–377, 2007.

[11] Nabielek and K. Verfondern, and H. Werner. *Can we predict coated particle failure?* A conversation on CONVOL, PANAMA and other codes. Technical Meeting on "Current Status and Future Prospects of Gas Cooled Reactor Fuels," IAEA, Vienna, 2004.

[12] Kidson, G. V., 1980, "A generalized analysis of the cumulative diffusional release of fission product gases from an 'equivalent sphere' of UO_2," *Journal of Nuclear Materials*, **88,** p. 299–308, 1980.

[13] Besmann, T. M., 2010, "Thermochemical assessment of oxygen gettering by SiC or ZrC in PuO_{2-x} TRISO fuel*,*" *Journal of Nuclear Materials*, **397**, p. 69–73, 2010.

[14] Smith, J. M., H. V. van Ness, and M. M. Abott, 2001, *Introduction to chemical engineering thermodynamics,* McGraw-Hill, ISBN 0-07-118957-2, 2001.

[15] Ho, F., 1993, "Material Models of Pyrocarbon and Pyrolytic Silicon Carbide*,*" Technical Report CEGA-002820, CEGA Corporation, San Diego, CA, 1993.

[16] Bacon, G. E., 1956, "A method for determining the degree of orientation of graphite," *Journal of Applied Chemistry*, **6**, p. 477–481, 1956.

[17] I-NERI. *Development for improved models and designs for coated particle gas reactor fuels*. Technical Report INEEL/EXT-05-02615, INEEL, 2004.

[18] Wang, J., 2004, *An integrated performance model for high temperature gas cooled reactor coated particle fuel,* PhD thesis, Massachusetts Institute of Technology, 2004.

[19] Bende, E. E., 1998, "Maximisation of the Doppler effect in thermal reactors*," International Conference on the Physics of Nuclear Science and Technology, New York, ANS, October 1998*.

[20] Bende, E. E., 2000, *Plutonium Burning in a Pebble-Bed Type High Temperature Reactor*, PhD thesis, TU-Delft, The Netherlands, 2000.

[21] van Dam, H., 2000, "Long-term control of excess reactivity by burnable particles," *Annals of Nuclear Energy* **27**, p. 733–743, 2000.

[22] Lohnert, G. H., 1990, "Technical Design Features and Essential Safety Related Properties of the HTR-MODULE," *Nuclear Engineering and Design*, **121**, 259–275, 1990.

[23] Zheng, Y., L. Shi, and Y. Dong, 2009, "Thermohydraulic transient studies of the Chinese 200 MWe HTR-PM for loss of forced cooling accidents," *Annals of Nuclear Energy*, **36**, 742–751, 2009.

[24] Zhang, Z., Z. Wu, D. Wang, Y. Xu, Y. Sun, F. Li, Y. Dong, 2009, "Current status and technical description of Chinese 2x 250 MW_{th} HTR-PM demonstration plant," *Nuclear Engineering and Design*, **239**: 1212–1219, 2009.

[25] Teuchert, E., U. Hansen, K. A. Haas, H. J. Rütten, H. Brockmann, H. Gerwin, U. Ohlig, W. Scherer, 1994, V.S.O.P.('94)-Computer Code System for Reactor Physics and Fuel Cycle Simulation – Input Manual and Comments, Forschüngszentrum Jülich, 1994.

[26] Kugeler, K., and R. Schulten, *Hochtemperaturreaktortechnik*, Springer-Verlag, 1989.

[27] Besmann, T. M., 2010, "Thermochemical assessment of oxygen gettering by SiC or ZrC in PuO_{2-x} TRISO fuel," *Journal of Nuclear Materials*, **397**, p. 69–73, 2010.

[28] Horsley, G. W., G. J. Weldrick, J. A. Turnbull and R. Shipp, 1976, Influence of Irradiation Temperature, Burnup, and Fuel Composition on Gas Pressure (Xe ,Kr,CO, CO_2) in Coated Particle Fuels," *Journal of the American Ceramic Society*, **59**, Number 1–2, 1976.

[29] Proksch, E., A. Strigl and H. Nabielek, 1982, "Production of carbon monoxide during burn-up of UO2 kerneled HTR fuel particles," *Journal of Nuclear Materials*, **107**, p. 280–285, 1982.

[30] Kim, Y. M., M. S. Cho, Y. W. Lee, W. J. Lee., 2008, "Development of a Fuel Performance Analysis Code COPA," *In Proceedings of the 4th International Topical Meeting on High Temperature Reactor Technology (HTR-2008). Washington D.C., USA, September–October 2008*.

[31] CEGA-002549, 1993, "PISA -Software Requirement Specifications for Code to Perform Mechanical Analysis of Irradiated Fuel Particles," Technical report, CEGA Corporation, 1993.

[32] CEGA-002550, 1993, *PISA: A Coupled Thermal-Stress Code for the Mechanical Analysis of Irradiated Fuel Particles* – User's Manual, Technical report, CEGA Corporation, 1993.

[33] Boer, B., Y. M. Kim, W. Wu, A. M. Ougouag, D. McEachern, F. Venneri, 2010, "Inter-comparison of Computer Codes for TRISO-based Fuel Micro-Modeling and Performance Assessment," *Proceedings of HTR 2010, Prague, Czech Republic, October 2010*.

[34] Boer, B., A. M. Ougouag, 2010, "Core Analysis, Design and Optimization of a Deep-Burn Pebble Bed Reactor." *In Proceedings of the PHYSOR 2010 -Advances in Reactor Physics to Power the Nuclear Renaissance. American Nuclear Society, Pittsburgh, USA, May 2010.*

[35] INERI, 2004, "Development of improved models and designs for coated-particle gas reactor fuels." Technical Report INEL/EXT-05-02615, Final report under the international nuclear energy research initiative, December 2004.